*J. metamorphic Geol.*, 2006, **24,** 329–347 doi:10.1111/j.1525-1314.2006.00641.x

# Two-stage metamorphic evolution of the Bemarivo Belt of northern Madagascar: constraints from reaction textures and *in situ* monazite dating

N. JÖNS,[1] V. SCHENK,[1] P. APPEL[1] AND T. RAZAKAMANANA[2]
[1]*Institut für Geowissenschaften, Christian-Albrechts-Universität, 24098 Kiel, Germany (nj@min.uni-kiel.de)*
[2]*Département des Sciences de la Terre, Université de Toliara, Toliara, Madagascar*

**ABSTRACT** New results on the pressure–temperature–time evolution, deduced from conventional geothermobarometry and *in situ* U-Th-total Pb dating of monazite, are presented for the Bemarivo Belt in northern Madagascar. The belt is subdivided into a northern part consisting of low-grade metamorphic epicontinental series and a southern part made up of granulite facies metapelites. The prograde metamorphic stage of the latter unit is preserved by kyanite inclusions in garnet, which is in agreement with results of the garnet (core)-alumosilicate-quartz-plagioclase (inclusions in garnet; GASP) equilibrium. The peak metamorphic stage is characterized by ultrahigh temperatures of ~900–950 °C and pressures of ~9 kbar, deduced from GASP equilibria and feldspar thermometry. In proximity to charnockite bodies, garnet-sillimanite-bearing metapelites contain aluminous orthopyroxene (max. 8.0 wt% $Al_2O_3$) pointing to even higher temperatures of ~970 °C. Peak metamorphism is followed by near-isothermal decompression to pressures of 5–7 kbar and subsequent near-isobaric cooling, which is demonstrated by the extensive late-stage formation of cordierite around garnet. Internal textures and differences in chemistry of metapelitic monazite point to a polyphasic growth history. Monazite with magmatically zoned cores is rarely preserved, and gives an age of *c.* 737 ± 19 Ma, interpreted as the maximum age of sedimentation. Two metamorphic stages are dated: M1 monazite cores range from 563 ± 28 Ma to 532 ± 23 Ma, representing the collisional event, and M2 monazite rims (521 ± 25 Ma to 513 ± 14 Ma), interpreted as grown during peak metamorphic temperatures. These are among the youngest ages reported for high-grade metamorphism in Madagascar, and are supposed to reflect the Pan-African attachment of the Bemarivo Belt to the Gondwana supercontinent during its final amalgamation stage. In the course of this, the southern Bemarivo Belt was buried to a depth of >25 km. Approximately 25–30 Myr later, the rocks underwent heating, interpreted to be due to magmatic underplating, and uplift. Presumably, the northern part of the belt was also affected by this tectonism, but buried to a lower depth, and therefore metamorphosed to lower grades.

**Key words:** East African Orogen; Gondwana assembly; Pan-African; U-Th-total Pb dating; ultrahigh-temperature metamorphism.

## INTRODUCTION

A fundamental method of reconstructing former geodynamic processes is by the determination of pressure–temperature–time paths of metamorphism. In polymetamorphic terranes, additional accurate *in situ* dating of metamorphic textures is particularly important to understand the often complicated tectono-thermal history. By integrating chronological and pressure–temperature information, better constraints on the timing of burial and exhumation during orogenic processes can be obtained.

The Neoproterozoic East African Orogen is one of the largest orogenic belts on Earth, extending from Arabia to the whole Eastern Africa into Antarctica (Fig. 1). It was formed during the Pan-African orogeny, which is considered to have caused the final assembly of the supercontinent Gondwana (McWilliams, 1981; Stern, 1994). In recent years, advances in dating techniques have led to more precise geochronologic results, which show that the formerly considered final collision between East and West Gondwana cannot be attributed to a single tectonic event (Meert *et al.*, 1995; Meert, 2003). In fact, it has to be assumed that the Pan-African orogeny consisted of a series of discrete events, the exact timing and local distribution of which are not always well known. Madagascar holds a central position in the East African Orogen (Fig. 1), because it preserves a section from an Archean craton, i.e. the Antongil Block (Fig. 2a), to the western orogenic hinterland. A tectonic subdivision has recently been proposed (Collins *et al.*, 2000b; Collins & Windley, 2002), but reliable data on the *P–T–t* evolution of the different units, especially in

 

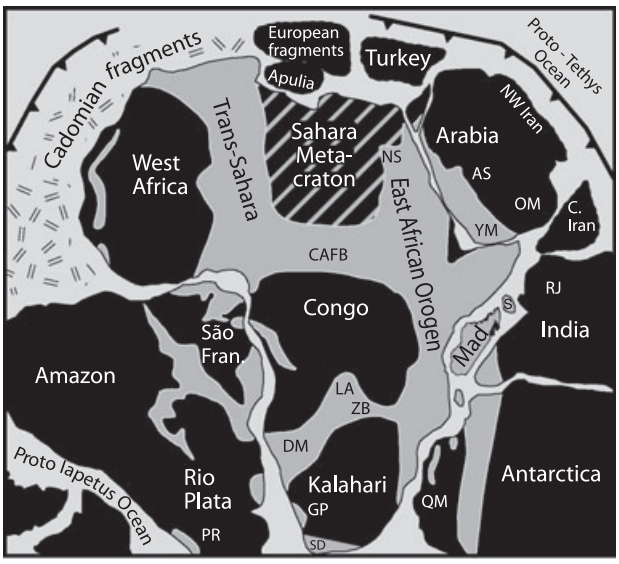


**Fig. 1.** Reconstruction of a part of the Gondwana supercontinent, at *c.* 544 Ma (modified after Kusky *et al.*, 2003, and references therein), showing the relationship between Madagascar and the surrounding areas. Pan-African orogens are marked in grey, cratons in black. AS, Arabian Shield; CAFB, Central African Fold Belt; GP, Gariep; DM, Damara; LA, Lufilian Arc; Mad, Madagascar; OM, Oman; PR, Pampean Ranges; PS, Paterson; QM, Queen Maud Land; RJ, Rajasthan; São Fran., São Francisco; SD, Saldania; S, Seychelles; YM, Yemen; NS, Nubian Shield; ZB, Zambezi Belt.

northern and central Madagascar, are mostly lacking. The Antongil Block (Fig. 2a) is believed to represent a part of the Indian Dharwar Craton. West of the Antongil Block, there is the ~2.5-Ga Antananarivo Block. Both are separated from each other by a 30- to 60-km-wide region, consisting of metasedimentary rocks with enclosed basic and ultrabasic rocks. This zone is interpreted as an oceanic suture, named the Betsimisaraka suture (Fig. 2a; Collins *et al.*, 2000b; Kröner *et al.*, 2000).

Up to now, not much attention has been paid to the role of the Bemarivo Belt in the formation of Gondwana. It is situated in northern Madagascar, just north of the cratonic Archean Antongil Block (Fig. 2a). On the basis of geochronology, as well as palaeogeographic continental reconstructions of Gondwana, it is correlated with the Seychelles and the Rajasthan region of India (Tucker *et al.*, 1999a; Torsvik *et al.*, 2001). Large areas within the Bemarivo Belt consist of metasedimentary rocks, which are suitable for applying conventional geothermobarometry. Here, we present new data and observations on the petrology of these rocks, in order to deduce the *P–T* conditions during the Pan-African orogeny. In addition, chemical U-Th-total Pb dating was undertaken on polyphase monazite to unravel the geodynamic evolution of this central part of Gondwana.

## GEOLOGICAL SETTING

The Bemarivo Belt is the northernmost basement unit of Madagascar. It strikes WNW–ESE and truncates structures in the Antananarivo Block, the Antongil Block and the Betsimisaraka suture zone (Fig. 2a). It can be subdivided into three distinct regions (Fig. 2b). The southern region is 50–150 km wide, extends from the area around Antalaha (in the east) to the Sambirano river (in the west) and consists of high-grade metapelitic rocks. It is bordered to the north by a 50- to 80-km-broad region, dominated by metagranitoids and granites. The northernmost part consists of lower-grade metamorphic epicontinental series. Following the established nomenclature for lithologies in southern Madagascar, Besairie (1970) attributed the southern area to the 'Système du Graphite', whereas the northern part belongs to the 'Système du Vohibory'. According to the geological synthesis of Madagascar after Hottin (1976), this southern area is termed the 'Séries de Sahantaha' and consists of kyanite- and sillimanite-bearing quartzites, micaschists, granites, conglomerates, paragneisses, marbles and minor amphibolites. Within this series, Hottin (1976) noted an increasing metamorphic grade from the Antongil Block (Système d'Antongil) towards the north and the west. The northern part is termed the 'Série de Daraina-Milanoa'. It consists of muscovite-bearing paragneisses, conglomerates, metavolcanics, quartzites, marbles, amphibolites and micaschists containing kyanite or garnet-staurolite. The grade of metamorphism is greenschist- to epidote-amphibolite facies.

The Bemarivo Belt is thought to represent a part of a Neoproterozoic continental arc terrane (Tucker *et al.*, 1999a; Buchwaldt & Tucker, 2001). A rhyolite of the Série de Daraina-Milanoa has been dated at *c.* 715 Ma (Tucker *et al.*, 1999a). A granitic intrusion in the migmatites of the central part formed at 753.8 ± 1.7 Ma (Tucker *et al.*, in Ashwal, 1997). Collins *et al.* (2000a) postulated an overthrusting of the Bemarivo Belt to the south after closure of the Betsimisaraka suture. Syntectonic metamorphism in the southern part of the Bemarivo Belt reached granulite facies grade at 520–510 Ma (Tucker *et al.*, 1999a; Buchwaldt *et al.*, 2003). Afterwards, extensional collapse is thought to have occurred (Collins *et al.*,

**Fig. 2.** Simplified geological map of northern Madagascar, modified after Besairie (1970) and Hottin (1976). (a) Overview over the main tectonic units of northern Madagascar (modified after Collins & Windley, 2002). To the west, the Archean Antongil Block is rimmed by the proposed Betsimisaraka suture zone. The Bemarivo Belt is crosscutting both units. (b) Map of the Bemarivo Belt, showing our sample localities. (c) Cutout of panel (b), showing the geology and sample locations of the area between Andapa and Sambava, as well as the position of the Massif de Marojezy.

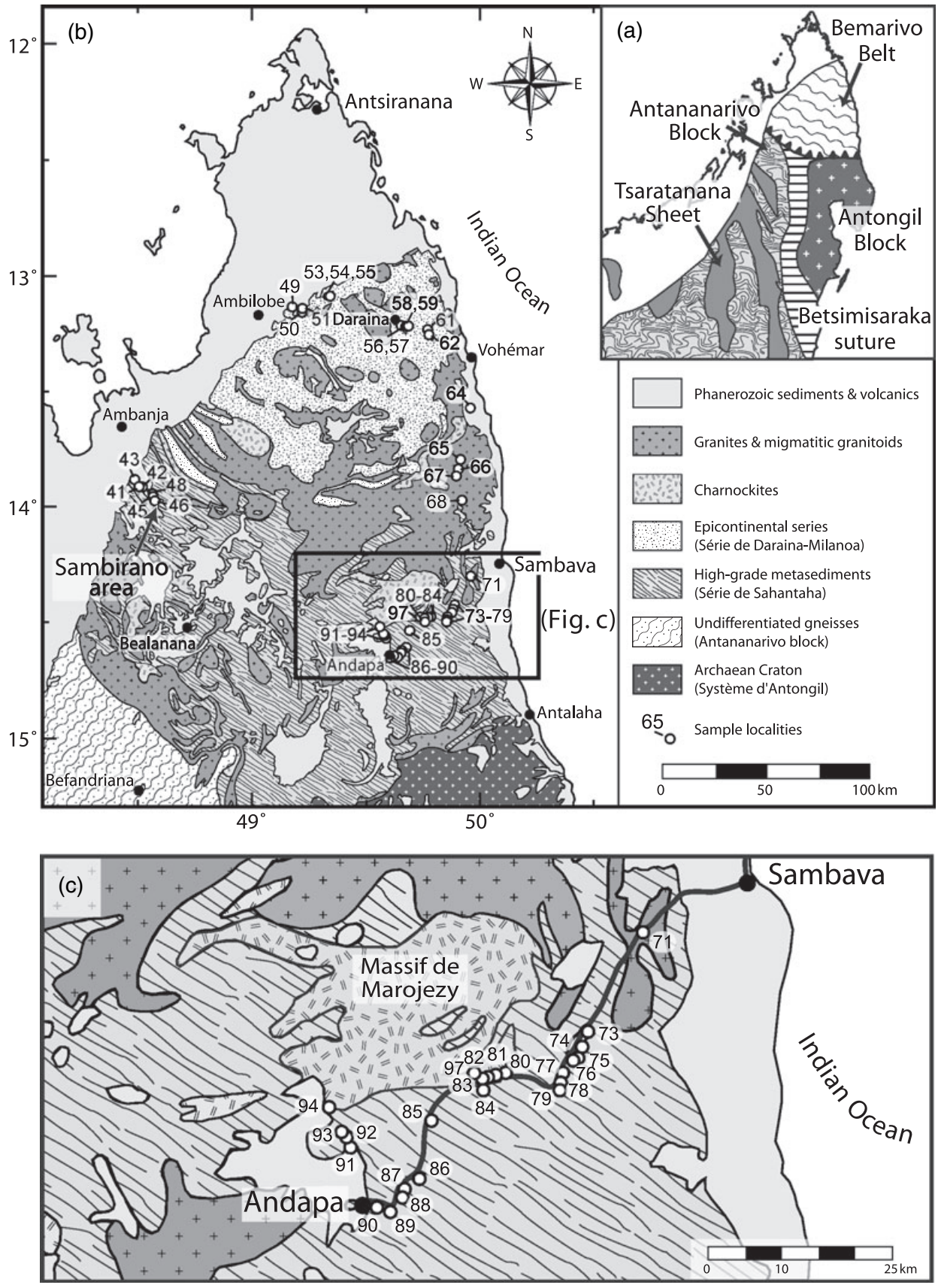

2000a). Conventional geothermobarometry has been applied by Buchwaldt *et al.* (2003) to rocks of the southern Bemarivo Belt. They determined metamorphic conditions of 750–930 °C and 6–10 kbar. However, their thermometric estimates are based only on Fe-Mg exchange between minerals, which is problematic for constraining conditions of high-$T$ metamorphic rocks because of re-equilibration on cooling (e.g. Fitzsimons & Harley, 1994).

In the southern part of the Bemarivo Belt, garnet-free enderbitic and charnockitic gneisses, which frequently show migmatization, are found (Fig. 3a). Other rock types, such as calcsilicates, marbles, quartzites and metabasites, occur just in small amounts. In the area between Sambava and Andapa (Fig. 2b,c), migmatitic metapelites (Fig. 3b) commonly occur, which are mostly lacking in the Sambirano area. In the northern part of the Bemarivo Belt, samples were taken along the roadside from Ambilobe via Daraina and Vohémar to Sambava (Fig. 2b). Samples are generally epidote-bearing amphibolites, but quartzites and muscovite-bearing micaschists also occur in minor amounts. Between Vohémar and Sambava, granitic and granodioritic gneisses are predominant.

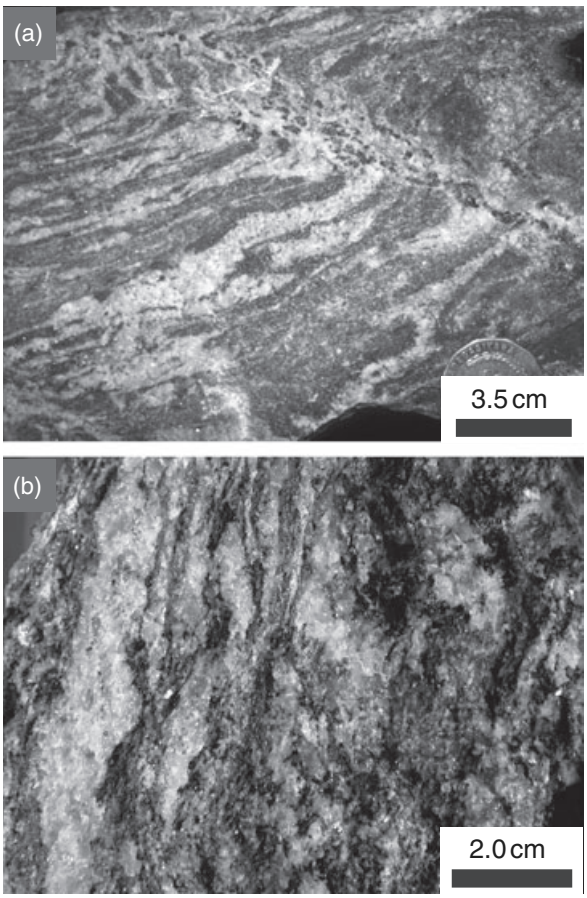


**Fig. 3.** (a) Enderbitic gneiss showing intense migmatization (Central Bemarivo Belt, Md65). (b) Metapelite containing leucosomes as well as biotite- and sillimanite-rich bands (Southern Bemarivo Belt, Md83).

## ANALYTICAL PROCEDURE AND DATA PROCESSING

Measurements were performed on a JEOL Superprobe JXA-8900R electron microprobe at the University of Kiel, equipped with five wavelength-dispersive spectrometers. The accelerating voltage was generally 15 kV for a probe current of 20 nA. Yttrium in garnet was measured with 20 kV and 300 nA; for apatite measurements (needed for Grt-Mnz thermometry) 10 kV and 10 nA were used. Synthetic and natural minerals were used as the standards. Sample spot sizes were 1–7 $\mu$m in diameter. The raw data were corrected using the CITZAF method of Armstrong (1995).

For feldspar thermometry, the composition of mesoperthitic grains was reintegrated from measurements of plagioclase and alkali-feldspar. The proportions of host and lamellae were determined from backscattered electron images using an image analysis software. The textural context of the grains was carefully checked to account for possible exsolution-free or recrystallized rims.

For monazite measurements, the accelerating voltage was 20 kV with a probe current of 80 nA. The following standard materials were used: synthetic orthophosphates (Jarosewich & Boatner, 1991) for P, Y and REE; synthetic uranium-bearing glass for U; natural wollastonite for Ca and Si; thorianite for Th; crocoite for Pb; corundum for Al. X-ray lines, measurement crystals and counting times are listed in Table 1. Matrix correction for monazite analyses was performed using the JEOL ZAF program. The interference of Th M$\gamma$ on U M$\beta$ was corrected with an experimentally derived correction factor.

**Table 1.** Measurement conditions for U-Th-total Pb dating of monazite.

| | | | Measurement time (s) | |
|---|---|---|---|---|
| Element | Crystal | Line | Peak | Background |
| U | PETH | M$\beta$ | 50 | 30 |
| Th | PETH | M$\alpha$ | 20 | 10 |
| Pb | PETH | M$\beta$ | 220 | 100 |
| P | PETJ | K$\alpha$ | 15 | 7 |
| Ca | PETH | K$\alpha$ | 15 | 5 |
| Si | TAP | K$\alpha$ | 40 | 20 |
| Y | PETJ | L$\alpha$ | 30 | 10 |
| Al | TAP | K$\alpha$ | 20 | 10 |
| Sm | LIF | L$\beta$ | 60 | 30 |
| La | LIF | L$\alpha$ | 60 | 30 |
| Eu | LIF | L$\beta$ | 30 | 10 |
| Ce | LIF | L$\alpha$ | 15 | 7 |
| Dy | LIF | L$\alpha$ | 100 | 30 |
| Nd | LIF | L$\alpha$ | 20 | 10 |
| Gd | LIF | L$\beta$ | 40 | 20 |
| Pr | LIF | L$\beta$ | 80 | 20 |
| Er | LIF | L$\alpha$ | 80 | 20 |

Background measurement time is given for one background.

All monazite was analysed *in situ* to have textural control over the mineral inclusion relationships. For control over internal zoning, backscattered electron images as well as X-ray maps of Y, Th, U and Pb were obtained. The samples were polished on Pb-free polishing discs. As an internal laboratory standard during measurements, the homogeneous monazite F6 from the Anosyan Massif (Manangotry Pass) in SE Madagascar (kindly provided by M. Raith, Bonn) was repetitively analysed. It was dated with the U-Pb method of cogenetic zircon and by a Sm-Nd monazite-biotite-garnet-zircon isochron at 545 ± 2 and 542 ± 11 Ma, respectively (Paquette *et al*., 1994). Analytical errors for each analysis were calculated from the counting statistics using the program 'CombError' of P. Appel (can be downloaded from http://www.min.uni-kiel.de/epma/sw.html). The age was calculated after the isochron method of Suzuki & Adachi (1991, 1994), using the software of Kato *et al*. (1999) with decay constants from Steiger & Jäger (1977). A York-regression isochron (York, 1966) was forced through the origin (Cocherie *et al*., 1998) with an error of 150 ppm at the point of zero $ThO_2^*$ and PbO.

## PETROGRAPHY AND MINERAL CHEMISTRY

### Northern (Série de Daraina-Milanoa) and central Bemarivo Belt

The northern Bemarivo Belt is dominated by metabasic rocks, which are interpreted as metamorphosed volcaniclastic sediments (Hottin, 1976). Coarse-grained titanite-, epidote- and garnet-bearing amphibolites are common, and locally they show a strong metasomatic overprint. Granodioritic and granitic gneisses, as well as muscovite-bearing quartzites and micaschists also occur. Kyanite is reported from quartzites (Lacroix, 1922), and Hottin (1976) described garnet-staurolite parageneses from micaschists. The central part of the belt is made up largely of granites and gabbros, as well as enderbitic and charnockitic gneisses. The gneisses show intensive migmatization (Fig. 3a) and are generally garnet-free (only one sample contains late-stage garnet). This either points to high temperatures or low pressures during metamorphism. Porphyritic hornblende-biotite gneisses are subordinate.

### Southern Bemarivo Belt (Série de Sahantaha)

#### *Metapelites*

Metapelitic rocks, which commonly show migmatitic textures (Fig. 3b), occur in the Andapa-Sambava region of the southern Bemarivo Belt (Fig. 2c) and near Bealanana (Besairie, 1970, Fig. 2b). The sample locations are shown in Fig. 2 and the equilibrium mineral assemblages of the samples are given in Table 2. According to their mineral content, three main types can be distinguished. The most common metapelites contain kyanite, sillimanite, garnet, K-feldspar, quartz, biotite and late-stage cordierite (no. [1] in Table 2). Other assemblages lack either garnet or plagioclase or cordierite or alumosilicate (no. [2], [3] & [4] in Table 2). A second group of rocks contain additional orthopyroxene and locally spinel (no. [5] & [6] in Table 2). Some samples lack sillimanite (no. [4] & [6] in Table 2) and are of semipelitic composition. Finally, in minor amounts, silica-undersaturated high Mg-Al metapelites were found close to the Massif de Marojezy (Fig. 2c), closely associated with other metapelitic rocks. They contain corundum and sapphirine, but are quartz-free (no. [7] in Table 2).

**Table 2.** Mineral assemblages in metapelitic and semipelitic rocks.

| | | | | | | | | | |
|---|---|---|---|---|---|---|---|---|---|
| [1] | Ky/Sil | Grt | Kfs | Qtz | ± Pl | Bt | – | (Crd) | (± Spl) |
| [2] | Ky/Sil | – | Kfs | Qtz | Pl | Bt | – | – | – |
| [3] | Ky/Sil | – | Kfs | Qtz | – | Bt | – | (Crd) | – |
| [4] | – | Grt | Kfs | Qtz | Pl | Bt | – | – | – |
| [5] | Ky/Sil | Grt | Kfs | Qtz | Pl | Bt | Opx | (Crd) | (Spl) |
| [6] | – | Grt | Kfs | Qtz | Pl | Bt | Opx | – | – |
| [7] | Ky/Sil | – | Kfs | – | Pl | Bt | – | Crd/(Crd) | (± Spr) |

Common accessory minerals: Ap, Mnz, Ilm, Rt, Spl; in [7] also Crn

| | |
|---|---|
| [1] | 73-1-03, 73-3-03, 75-1-03, 76-1-03, 82-2-03, 83-1-03, 83-9-03, 83-10-03, 83-12-03, 83-14-03, 83-15-03, 84-1-03, 86-1-03, 87-1-03, 87-2-03, 88-1-03, 88-2-03, 88-3-03, 89-1-03, 90-1-03, 93-1-03, 93-2-03, 93-4-03 |
| [2] | 78-2-03 |
| [3] | 89-2-03 |
| [4] | 48-1-03, 80-1-03, 92-1-03 |
| [5] | 83-13-03 |
| [6] | 81-1-03, 81-2-03 |
| [7] | 83-2-03, 83-3-03, 83-4-03, 83-5-03, 83-6-03, 83-7-03, 83-8-03, M97-12-2 |

[1]–[4] are typical metapelitic rocks, [5] and [6] are rare Opx-bearing assemblages, and [7] are silica-undersaturated metapelites.

The metapelites of the first type are porphyroblastic, medium-grained, and show a well-developed schistosity made up of bands of sillimanite and biotite. Concordant as well as discordant leucosomes are frequently present (Fig. 3b). Garnet locally contains inclusions of kyanite near the core (Fig. 4a) and sillimanite needles close to the rim. Sillimanite in the matrix forms euhedral crystals (Fig. 4a), but large aggregates that are fine fibrous and undulously extinguishing are also very common (Fig. 4b). As a result of this texture, we interpret them as pseudomorphs formed after kyanite. Apart from a narrow retrograde re-equilibrated rim, even large garnet porphyroblasts are just weakly zoned (Fig. 5a), whereas smaller ones are unzoned. They have an $X_{Mg}$ [=Mg/(Mg + $Fe^{2+}$)] of 0.25–0.35, $X_{Prp}$ = 0.15–0.35, $X_{Alm}$ = 0.55–0.80, $X_{Sps}$ = 0.00–0.01 and $X_{Grs}$ = 0.02–0.03. Garnet cores have slightly higher grossular contents (~0.05) and lower $X_{Mg}$. Representative garnet analyses are given in Table 3. Brownish biotite forms hypidiomorphic flakes in the rock matrix (Fig. 4b,d). Coexisting with ilmenite or ilmenite + rutile, it has variable $X_{Mg}$ values of 0.35–0.60 and Ti contents of 0.4–0.7 p.f.u. (calculation based on 22 oxygen; Fig. 6a; Table 4). Some grains of

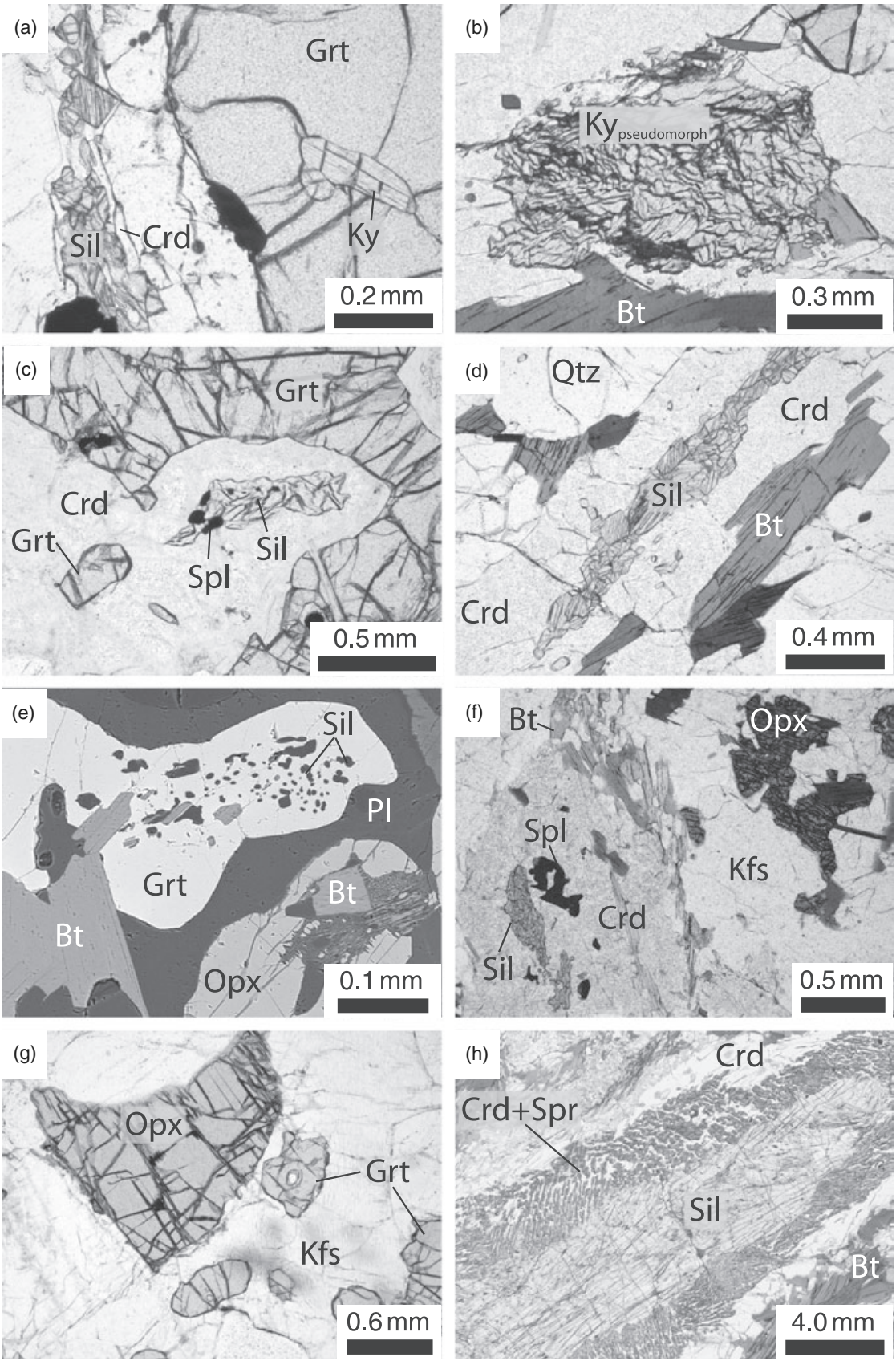

green late-stage biotite have much lower Ti contents (~0.2–0.3 p.f.u.). Cordierite forms rims around garnet (Fig. 4c) and separates biotite and sillimanite (Fig. 4d), and $X_{Mg}$ varies in the range of 0.6–0.8 (Table 4). All cordierite seems to have formed during retrograde metamorphism, and no inclusions of cordierite in garnet have been found. The large regional variation in the composition of garnet, biotite and cordierite is correlated with a systematic shift to the more Mg-rich side (Fig. 6b) from the SE to the NW of the Andapa area. Besides quartz, the matrix of the rock is mainly made up of alkalifeldspar ($X_{Or} = 0.8$–$0.9$). Plagioclase is inversely zoned and has a composition of $X_{An} = 0.2$–$0.3$ in the core and $X_{An} = 0.3$–$0.4$ at the rim (Table 5). Some metapelites contain plagioclase with $X_{An} = 0.55$–$0.60$ and inclusions in garnet with even higher $X_{An}$ of 0.65–0.70. Reintegrated compositions of mesoperthitic feldspar are shown in Fig. 7. Common accessory minerals are monazite and zircon, which occur in the rock matrix as well as inclusions in garnet. Apatite has just been found to be included in garnet. Cordierite- and sillimanite-free garnet-biotite gneisses (no. [4] in Table 2) occur in the whole southern Bemarivo Belt. Garnet and biotite form porphyroblasts in a rock matrix consisting of quartz and mesoperthitic feldspar (Fig. 7). A sample from the Sambirano area (48-1-03) contains garnet with $X_{Mg} = 0.22$–$0.26$, $X_{Prp} = 0.21$–$0.24$, $X_{Alm} = 0.68$–$0.71$, $X_{Sps} = 0.05$–$0.06$ and $X_{Grs} = 0.02$–$0.04$. Biotite is characterized by $X_{Mg} = 0.45$–$0.48$ and Ti contents of 0.60–0.67 p.f.u. (calculation based on 22 oxygen).

Garnet-orthopyroxene-sillimanite-bearing gneisses (no. [5] in Table 2) are found close the the Massif de Marojezy. Garnet porphyroblasts are strongly resorbed, and in few cases inclusions of sillimanite are present (Fig. 4e). Garnet is unzoned with $X_{Mg} = 0.25$–$0.30$, $X_{Prp} = 0.25$–$0.35$, $X_{Alm} = 0.65$–$0.70$, $X_{Sps} < 0.05$ and $X_{Grs} < 0.05$. The coexisting orthopyroxene (Fig. 4e,f) is up to 2 mm in diameter and has a constant $X_{Mg}$ of 0.60–0.65. The alumina content varies from 8 wt% in the core to 4.5 wt% near the rim (Fig. 5b; Table 5). Sillimanite is also preserved as aggregates, which are surrounded by late-stage cordierite ($X_{Mg} = 0.79$–$0.82$; Fig. 4f). Furthermore, biotite ($X_{Mg} = 0.65$–$0.67$; Ti = 0.38–0.46 p.f.u., based on 22 oxygen), quartz, mesoperthitic feldspar and late-stage spinel occur. Spinel has an $X_{Mg}$ of 0.29–0.34 (containing some $Fe^{3+}$) and is Zn-bearing (1.7–2.1 wt% ZnO). In sillimanite-free rocks (no. [6] in Table 2) garnet and orthopyroxene occur in leucosomes (Fig. 4g). Here, the pyroxene is unzoned with $X_{Mg} = 0.59$–$0.60$ and $Al_2O_3 = 4.2$–$5.5$ wt%. Garnet has a composition of $X_{Mg} = 0.30$–$0.45$, $X_{Prp} = 0.30$–$0.37$, $X_{Alm} = 0.48$–$0.64$, $X_{Sps} = 0.03$–$0.04$ and $X_{Grs} = 0.00$–$0.03$. Other minerals are quartz, plagioclase, alkalifeldspar and biotite (Fig. 6).

The matrix of the quartz-free high Mg-Al gneisses (no. [7] in Table 2) is composed of biotite ($X_{Mg} = 0.85$; Ti = 0.20–0.28 p.f.u.; Fig. 6a; Table 4), perthitic K-feldspar and euhedral cordierite ($X_{Mg} = 0.90$–$0.92$; Table 4). Cordierite of the same composition and mostly peraluminous sapphirine (Figs 4h & 5c; Table 4; $X_{Mg} = 0.86$–$0.89$ with ~5–15% of the total iron as $Fe_2O_3$) constitute symplectitic intergrowths, which separate sillimanite from the rock matrix (Fig. 4h). Fibrous fine-grained sillimanite forms large aggregates (up to 5 cm), which locally recrystallized to form a second generation of idiomorphic sillimanite. Some small grains of plagioclase are obviously derived from exsolution of perthites. Corundum is also present (not shown in Fig. 4h), either as fine needles included in sillimanite or as larger prismatic grains in cordierite of the matrix. In domains containing no sapphirine, the amount of corundum is higher.

### *Enderbitic and charnockitic gneisses*

Charnockitic gneisses form large complexes in the northern Sambirano as well as in the Andapa region. Their gneissic texture indicates deformation and metamorphism subsequent to emplacement. They are generally garnet-free and contain orthopyroxene. Locally, orthopyroxene is surrounded by late-stage clinopyroxene and biotite, the formation of which is attributed to cooling. Just in one charnockitic sample from the central Bemarivo Belt, late-stage spongy garnet has been found, most likely also grown during cooling. Common accessory minerals are apatite, monazite and zircon. Enderbitic gneisses consist of hornblende, orthopyroxene, clinopyroxene, plagioclase and accessory apatite, but do not contain garnet.

### *Other rock types*

Marbles, calcsilicates, ultrabasites and quartzites are subordinate in volume. Marbles consist of calcite, dolomite and minor amounts of phlogopite. Some small grains of forsterite are rimmed by diopside or tremolite. Calcsilicates are rich in titanite. Additional

**Fig. 4.** Microphotographs showing reaction textures in metapelites (mineral abbreviations after Kretz, 1983). Pictures are taken under plane-polarized light, except for panel e, which is a backscattered-electron image. (a) Garnet porphyroblast including kyanite, and sillimanite growing in the rock matrix (Md90-1-03). (b) Aggregate of sillimanite, interpreted as a pseudomorph after kyanite (Md75-1-03). (c) Garnet breakdown and late-stage formation of cordierite. Small relics of garnet are situated in the cordierite (Md83-14-03). (d) Cordierite rim separating biotite and sillimanite (Md88-3-03). (e) Coexisting garnet and orthopyroxene in a metapelite. Garnet contains inclusions of sillimanite (Md83-13-03). (f) Orthopyroxene porphyroblasts and sillimanite in a metapelitic rock. Sillimanite is surrounded by late-stage cordierite and spinel (Md83-13-03). (g) Orthopyroxene and garnet in the leucosome of a metapelitic gneiss (Md81-1-03). (h) Sillimanite mantled by a symplectite of cordierite and sapphirine (Md83-2-03).

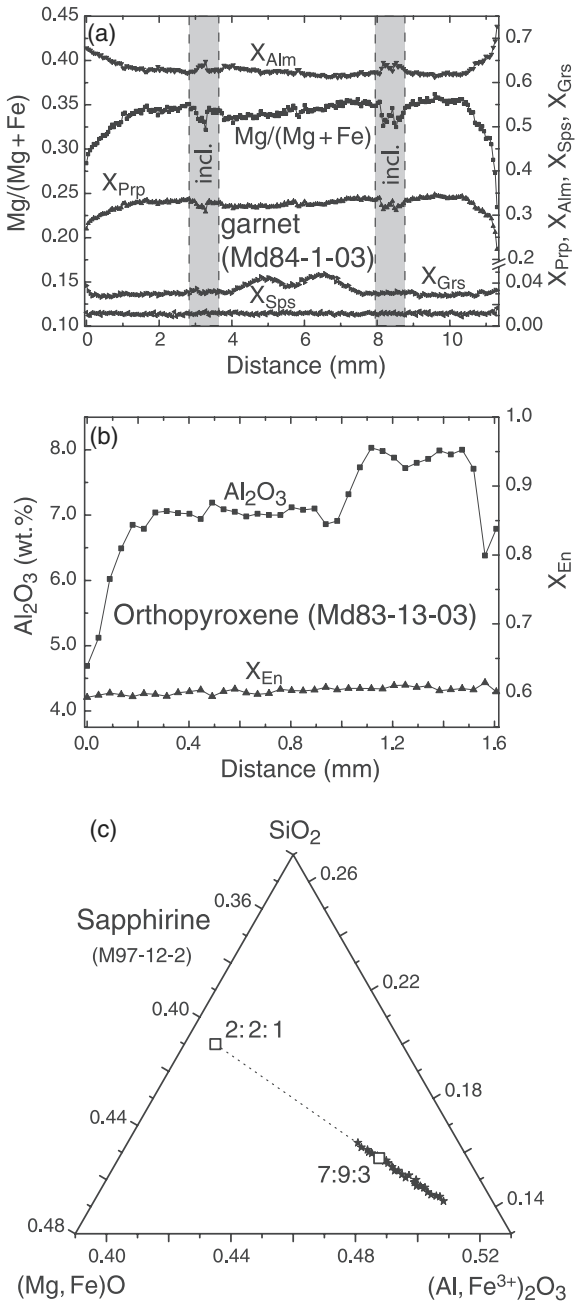


**Fig. 5.** (a) Chemical profile of a metapelitic garnet from a Grt-Sil-Bt-Crd gneiss, showing a weak zonation. The shaded areas are inclusion-rich (Bt, Kfs). (b) Profile through a metamorphic orthopyroxene (coexisting with Grt and Sil). A zonation in the alumina content is preserved, whereas the Mg-Fe is completely reequilibrated. (c) Sapphirine analyses in the diagram $(Mg,Fe)O–(Al,Fe^{3+})_2O_3–SiO_2$. For comparison, 7:9:3 and 2:2:1 compositions are shown (cf. Higgins *et al.*, 1979).

minerals are plagioclase, amphibole, diopside and scapolite. Ultrabasites occur as small lenses embedded in charnockites. They consist of amphibole, spinel, orthopyroxene and some plagioclase. Quartzites are nearly pure, except for some sillimanite and biotite.

## MINERAL REACTION HISTORY

Information about the *P–T* conditions during the prograde history of metapelites of the Bemarivo Belt is well documented by kyanite inclusions in garnet (Fig. 4a). Aggregates of near-coaxial sillimanite prisms in the rock matrix, which are clearly distinct from late euhedral crystals, are interpreted to be a pseudomorphic replacement after kyanite (Fig. 4b). As a result of the large amount of these fine-grained pseudomorphs in the matrix of the rocks, we conclude that at one stage of the evolution the rocks were well equilibrated in the kyanite stability field. Another common texture is the dehydration of biotite and formation of omnipresent leucosomes, which can be explained by the dehydration reaction

$$Bt + Sil + Pl + Qtz \rightleftharpoons Grt + Kfs + L. \quad (1)$$

In orthopyroxene-bearing rocks (no. [5] & [6] in Table 2), the dehydration was due to the reaction

$$Bt + Qtz \rightleftharpoons Opx + Grt + Kfs + L. \quad (2)$$

explaining the garnet- and orthopyroxene-bearing leucosomes (Fig. 4g). As a result of a decompressional stage, broad and well-equilibrated cordierite rims have formed around garnet (Fig. 4c; no. [1] in Table 2), locally leading to complete consumption of the garnet via the reactions

$$Grt + Sil + Qtz \rightleftharpoons Crd \quad (3)$$

$$Grt + Sil + L. \rightleftharpoons Crd + Kfs \quad (4)$$

The formation of cordierite is much more pronounced than in other areas that also show decompressional textures, such as Calabria or Sri Lanka (Schenk, 1984; Raase & Schenk, 1994). This indicates a decompressional stage either at higher temperatures or of longer duration than in other areas. In orthopyroxene + sillimanite-bearing rocks (no. [5] in Table 2) as well as orthopyroxene-free metapelites (no. [1] in Table 2), the formation of late-stage spinel and cordierite (Fig. 4f) reflects the reactions

$$Grt + Sil \rightleftharpoons Spl + Crd \quad (5)$$

$$Bt + Sil \rightleftharpoons Crd + Spl + Kfs + L. \quad (6)$$

In the rocks containing sapphirine (no. [7] in Table 2), the formation of cordierite most likely resulted from the breakdown of sillimanite + biotite:

$$Bt + Sil \rightleftharpoons Crd + Spr + Kfs \pm L. \quad (7)$$

Sapphirine–cordierite intergrowths are a typical texture in silica-undersaturated rocks and are interpreted to form during decompression (Kelsey *et al.*, 2005, and references therein). Finally, subsequent rehydration and cooling are texturally evidenced by the late-stage formation of greenish biotite and biotite–quartz intergrowths replacing cordierite. The fluid for this rehydration may be either of external

**Table 3.** Representative electron microprobe analyses of metapelitic garnet.

| Sample No. | 90-1 40* | 90-1 12* | 90-1 334* | 90-1 336* | 90-1 411† | 90-1 412† | 83-13 39† | 83-13 40† | 83-13 89* | 83-13 96* | 82-2 29† | 84-1 774‡ | 84-1 776‡ |
|---|---|---|---|---|---|---|---|---|---|---|---|---|---|
| $SiO_2$ | 38.88 | 38.97 | 38.81 | 38.77 | 38.73 | 39.08 | 38.34 | 38.79 | 38.52 | 38.78 | 37.94 | 38.27 | 38.02 |
| $TiO_2$ | 0.04 | 0.03 | 0.01 | 0.04 | 0.03 | 0.01 | 0.02 | 0.00 | 0.00 | 0.02 | 0.00 | 0.04 | 0.00 |
| $Al_2O_3$ | 21.87 | 21.81 | 21.87 | 21.94 | 21.78 | 21.93 | 21.91 | 21.87 | 21.92 | 22.08 | 21.54 | 21.20 | 21.11 |
| $Cr_2O_3$ | 0.03 | 0.04 | 0.03 | 0.03 | 0.02 | 0.04 | 0.03 | 0.02 | 0.02 | 0.04 | 0.11 | 0.01 | 0.03 |
| FeO | 28.36 | 28.88 | 27.76 | 27.97 | 29.10 | 28.60 | 31.72 | 30.88 | 30.81 | 29.99 | 34.48 | 32.63 | 32.50 |
| MgO | 9.06 | 9.06 | 8.09 | 8.18 | 9.08 | 9.00 | 6.81 | 7.70 | 7.73 | 7.79 | 5.67 | 6.31 | 6.11 |
| MnO | 0.35 | 0.32 | 0.30 | 0.29 | 0.36 | 0.31 | 1.29 | 1.29 | 1.15 | 1.18 | 0.26 | 0.68 | 0.77 |
| CaO | 1.26 | 1.16 | 3.05 | 2.81 | 0.89 | 0.82 | 0.56 | 0.58 | 0.57 | 0.55 | 0.60 | 1.09 | 1.20 |
| $Na_2O$ | n.d. | n.d. | n.d. | n.d. | n.d. | n.d. | n.d. | n.d. | n.d. | n.d. | n.d. | 0.02 | 0.05 |
| $Y_2O_3$ | 0.02 | 0.03 | n.d. | n.d. | n.d. | n.d. | n.d. | n.d. | n.d. | n.d. | n.d. | 0.02 | 0.05 |
| Total | 99.87 | 100.30 | 99.92 | 100.03 | 99.99 | 99.79 | 100.68 | 101.13 | 100.72 | 100.43 | 100.60 | 100.25 | 99.79 |
| Si | 3.00 | 3.00 | 3.00 | 3.00 | 3.00 | 3.02 | 2.99 | 3.00 | 2.99 | 3.00 | 2.99 | 3.01 | 3.01 |
| Ti | 0.00 | 0.00 | 0.00 | 0.00 | 0.00 | 0.00 | 0.00 | 0.00 | 0.00 | 0.00 | 0.00 | 0.00 | 0.00 |
| Al | 1.99 | 1.98 | 1.99 | 2.00 | 1.99 | 2.00 | 2.01 | 1.99 | 2.00 | 2.02 | 2.00 | 1.97 | 1.97 |
| Cr | 0.00 | 0.00 | 0.00 | 0.00 | 0.00 | 0.00 | 0.00 | 0.00 | 0.00 | 0.00 | 0.01 | 0.00 | 0.00 |
| Fe | 1.83 | 1.86 | 1.80 | 1.81 | 1.88 | 1.85 | 2.07 | 2.00 | 2.00 | 1.94 | 2.27 | 2.15 | 2.15 |
| Mg | 1.04 | 1.04 | 0.93 | 0.94 | 1.05 | 1.04 | 0.79 | 0.89 | 0.89 | 0.90 | 0.67 | 0.74 | 0.72 |
| Mn | 0.02 | 0.02 | 0.02 | 0.02 | 0.02 | 0.02 | 0.09 | 0.08 | 0.08 | 0.08 | 0.02 | 0.05 | 0.05 |
| Ca | 0.10 | 0.10 | 0.25 | 0.23 | 0.07 | 0.07 | 0.05 | 0.05 | 0.05 | 0.05 | 0.05 | 0.09 | 0.10 |
| Na | n.d. | n.d. | n.d. | n.d. | n.d. | n.d. | n.d. | n.d. | n.d. | n.d. | n.d. | 0.00 | 0.01 |
| Y | 0.00 | 0.00 | n.d. | n.d. | n.d. | n.d. | n.d. | n.d. | n.d. | n.d. | n.d. | 0.00 | 0.01 |
| Total | 7.98 | 8.00 | 7.99 | 8.00 | 8.01 | 8.00 | 8.00 | 8.01 | 8.01 | 7.99 | 8.01 | 8.01 | 8.02 |
| $X_{Mg}$ | 0.36 | 0.36 | 0.34 | 0.34 | 0.36 | 0.36 | 0.28 | 0.31 | 0.31 | 0.32 | 0.23 | 0.26 | 0.25 |
| $X_{Prp}$ | 0.35 | 0.34 | 0.31 | 0.31 | 0.35 | 0.35 | 0.26 | 0.29 | 0.30 | 0.30 | 0.22 | 0.24 | 0.24 |
| $X_{Alm}$ | 0.61 | 0.62 | 0.60 | 0.60 | 0.62 | 0.62 | 0.69 | 0.66 | 0.66 | 0.66 | 0.76 | 0.71 | 0.71 |
| $X_{Sps}$ | 0.01 | 0.01 | 0.01 | 0.01 | 0.01 | 0.01 | 0.03 | 0.03 | 0.03 | 0.03 | 0.01 | 0.02 | 0.02 |
| $X_{Grs}$ | 0.03 | 0.03 | 0.08 | 0.08 | 0.02 | 0.02 | 0.02 | 0.02 | 0.01 | 0.01 | 0.01 | 0.03 | 0.03 |

Cations calculated on the basis of 12 oxygen; *core analysis; †outer zone analysis; ‡rim analysis.

origin or may be derived from crystallizing anatectic melts.

In olivine-bearing marbles, forsterite is rimmed by diopside or tremolite, interpreted as due to the reactions

$$\mathrm{Fo} + \mathrm{Cal} + \mathrm{CO_2} \rightleftharpoons \mathrm{Di} + \mathrm{Dol} \quad (8)$$

$$\mathrm{Fo} + \mathrm{Cal} + \mathrm{CO_2} + \mathrm{H_2O} \rightleftharpoons \mathrm{Tr} + \mathrm{Dol} \quad (9)$$

The occurrence of both reactions reflects lowering of the $X_{CO_2}$ during cooling to $< 700$ °C (Käse & Metz, 1980).

## CONVENTIONAL GEOTHERMOBAROMETRY

The petrographic textures and mineral chemical data described above represent a robust frame for the clockwise character of the *P–T* evolution and the ultrahigh temperatures of metamorphism: kyanite inclusions in the core of garnet are the oldest relics of the metamorphic evolution in the metapelites. Thus, garnet growth started within the stability field of kyanite and proceeded in the sillimanite stability field. The omnipresence of pseudomorphic aggregates of sillimanite replacing former kyanite is evidence for an early metamorphic stage that led to the formation of the rocks, which were well equilibrated in the kyanite stability field. The ubiquitous occurrence of mesoperthitic feldspar in the southern Bemarivo Belt and the local occurrence of aluminous orthopyroxene coexisting with garnet and sillimanite point to the peak metamorphic temperatures exceeding 900 °C. The Ti-rich composition of biotite from all rock types confirms the suggestion of high-grade metamorphic conditions in the southern Bemarivo Belt. The extensive development of late-stage cordierite rims around garnet supports the interpretation of decompression under high temperatures.

In the following, results of conventional thermobarometry are presented to better constrain the *P–T* conditions during the different metamorphic stages. Geothermobarometric calculations were performed on metapelites of the southern Bemarivo Belt, especially on rocks from the area around Andapa. Mineral analyses used for *P–T* calculations are given in Tables 2–4; results are shown in Tables 6, 7 and Fig. 8. Garnet–monazite thermometry (Pyle *et al.*, 2001) using Y-rich garnet cores (200–300 ppm) and inclusions of monazite ($X_{YPO_4} = 0.010$–$0.035$), Ca-rich plagioclase ($X_{An} = 0.3$–$0.5$) and fluorine-rich apatite ($X_F = 0.70$–$0.85$; $X_{OH} = 0.10$–$0.25$; ($X_{Cl} \approx 0.05$) gives prograde temperature estimates in the range 560–585 °C (at 6.0 kbar, assumed $fH_2O = 1600$ bar). Garnet also contains inclusions of kyanite, therefore the garnet-alumosilicate-quartz-plagioclase (GASP) geobarometer has been applied for pressure estimates. Using the calibration of Koziol (1989), analyses of garnet cores and Ca-rich plagioclase inclusions in garnet ($X_{An} = 0.40$) give prograde pressure results in the stability field of kyanite (~6 kbar at 550 °C). If the Ca content in garnet cores is not the one that formed during garnet growth but is lower because of partial re-equilibration

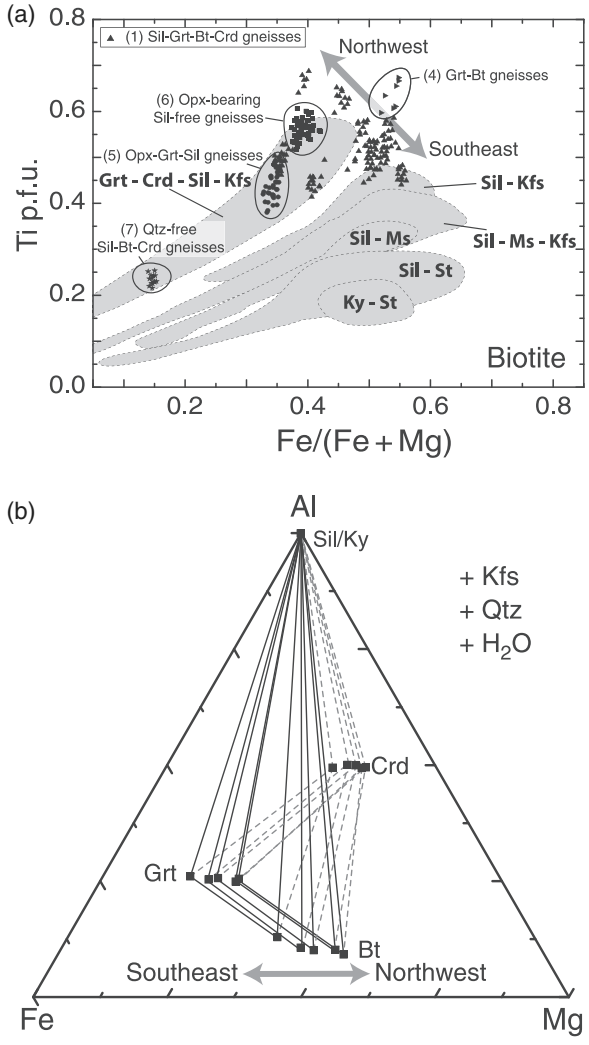


**Fig. 6.** (a) Compositions of metapelitic biotite from rocks of the southern Bemarivo Belt in the $X_{Fe}$ *v.* Ti p.f.u. diagram (formula units calculated on the basis of 22 oxygen; coexisting with ilmenite or ilmenite + rutile). Most biotite (triangular symbols) is from Grt-Sil-Bt-Crd gneisses and shows a systematic change in chemical composition from south-east to north-west. Biotite analyses from other metapelitic mineral assemblages are also shown (numbers refer to Table 2). Shaded fields: compositional ranges of biotite from metamorphic zones in New England (Robinson *et al.*, 1982). (b) AFM diagram (projection from Kfs, Qtz and $H_2O$) showing mineral compositions of Grt-Sil-Bt-Crd gneisses from the Andapa area. The gradual increase of Mg contents towards the north-west points to increasing metamorphic conditions.

by intracrystalline diffusion during peak temperatures, the obtained prograde GASP pressure estimates may represent only minimum pressure values for the early metamorphic stage. Outer zone analyses of garnet and matrix plagioclase ($X_{An} = 0.31$) give estimates for peak metamorphic pressure values of ~8.5 kbar (at 950 °C), in agreement with the omnipresence of matrix sillimanite. Peak temperatures are calculated from orthopyroxene-bearing metapelites using the Al-in-Opx thermometer of Harley & Green (1982). Results for orthopyroxene cores (up to 8 wt% $Al_2O_3$) and garnet are in the range of 950–1000 °C (at 8.5 kbar), which is in agreement with Al-isopleths of Harley & Motoyoshi (2000, Fig. 8). The combination of GASP (outer garnet zone/matrix plagioclase) with feldspar thermometry of metapelitic rocks yields estimates for the peak of metamorphism of ~950 °C at 9 kbar, which is at slightly lower temperatures than the results from orthopyroxene-bearing samples. However, just one alumosilicate-bearing metapelitic sample contains orthopyroxene, and this sample occurs close to the Massif de Marojezy. Therefore, temperature estimates on this sample may reflect just local conditions. But widespread high temperatures are supported by feldspar thermometry. Mesoperthites in an orthopyroxene-bearing metapelite (Md83-13-03) yield minimum temperatures of approximately 940 °C, which is in fair agreement with results of Al-in-Opx thermometry applied to the same sample. To avoid determining a magmatic rather than a metamorphic temperature, ternary feldspars of metapelitic rocks were examined. Reintegrated compositions of these mesoperthites point to minimum metamorphic temperatures of ~900–950 °C (Fig. 7a, Table 7). Feldspar in a metaigneous sample (Md94-2-03) taken close to the Marojezy massif yields slightly higher temperatures of ~980 °C. A decompression to ~6 kbar (at 850 °C) following a near-isothermal path is deduced from Al-in-Opx using garnet and orthopyroxene rims (coexisting with sillimanite) and from garnet-cordierite-sillimanite-quartz equilibria (Berman & Aranovich, 1996; with Berman, 1991). Using the outermost re-equilibrated rims of garnet and the neighbouring cordierite, Grt-Crd Fe-Mg exchange thermometry (Berman & Aranovich, 1996; with Berman, 1991) leads to ~650 °C (Table 6; Fig. 8). This temperature has to be interpreted as the closing temperature of the Fe-Mg exchange between both minerals. Further evidence for the cooling stage is given by the formation of late-stage garnet in one charnockitic gneiss sample. However, this sample is from the central part of the Bemarivo Belt, and a correlation with the metamorphic conditions of the metapelites in the southern part of the belt is not unequivocal.

## GEOCHRONOLOGY

For the geodynamic interpretation of the evolution of metamorphic rocks, it is of particular importance to correlate metamorphic reaction textures with the ages of the corresponding metamorphic events. Monazite is the best mineral for dating metamorphism in pelitic lithologies, because it occurs frequently and nearly all included pb is radiogenic (Parrish, 1990; Montel *et al.*, 1994). In addition, internal zoning can record significant details of the metamorphic history, e.g. several distinct growth events. Here, the method of chemical dating of monazite using electron microprobe analyses (U-Th-total Pb dating) was used. Although the preci-

**Table 4.** Representative electron microprobe analyses of metapelitic biotite, sapphirine, and cordierite.

| Sample No. | 81-1 Bt (602) | 90-1 Bt (40) | 48-1 Bt (5) | 93-2 Bt (14) | M97/12 Bt (645) | M97/12 Spr (449) | M97/12 Spr (454) | 82-2 Crd (20)* | 84-1 Crd (826)* | 84-1 Crd (819)‡ | 84-1 Crd (823)‡ | M97/12 Crd (304) |
|---|---|---|---|---|---|---|---|---|---|---|---|---|
| $SiO_2$ | 35.84 | 35.58 | 36.19 | 36.30 | 39.61 | 11.96 | 12.31 | 49.39 | 48.59 | 49.04 | 49.16 | 50.72 |
| $TiO_2$ | 5.04 | 5.62 | 5.19 | 5.82 | 2.52 | 0.01 | 0.08 | 0.00 | 0.00 | 0.02 | 0.00 | 0.02 |
| $Al_2O_3$ | 16.53 | 15.72 | 14.73 | 15.44 | 17.76 | 65.67 | 65.36 | 32.48 | 32.36 | 32.31 | 32.27 | 32.59 |
| $Cr_2O_3$ | 0.06 | 0.00 | 0.00 | 0.00 | 0.05 | 0.03 | 0.03 | 0.00 | 0.02 | 0.00 | 0.04 | 0.00 |
| FeO | 15.12 | 16.85 | 19.35 | 15.04 | 5.80 | 3.97 | 4.39 | 6.08 | 5.92 | 5.48 | 5.73 | 2.01 |
| $Fe_2O_3$ | n.c. | n.c. | n.c. | n.c. | n.c. | 0.91 | 0.46 | n.c. | n.c. | n.c. | n.c. | n.c. |
| MgO | 12.73 | 11.26 | 10.03 | 12.62 | 20.24 | 17.06 | 17.16 | 9.64 | 9.88 | 10.09 | 9.94 | 12.50 |
| MnO | 0.06 | 0.00 | 0.10 | 0.00 | 0.00 | 0.11 | 0.11 | 0.03 | 0.05 | 0.09 | 0.03 | 0.08 |
| CaO | 0.00 | 0.00 | 0.11 | 0.00 | 0.00 | 0.02 | 0.01 | 0.00 | 0.00 | 0.02 | 0.00 | 0.00 |
| $Na_2O$ | 0.06 | 0.09 | 0.16 | 0.17 | 0.14 | 0.02 | 0.02 | 0.08 | 0.11 | 0.08 | 0.07 | 0.13 |
| $K_2O$ | 10.20 | 10.09 | 10.03 | 10.11 | 9.81 | 0.01 | 0.00 | 0.00 | 0.00 | 0.00 | 0.01 | 0.01 |
| BaO | n.d. | n.d. | 0.11 | n.d. | n.d. | 0.00 | 0.00 | n.d. | n.d. | n.d. | n.d. | n.d. |
| $P_2O_5$ | n.d. | n.d. | n.d. | n.d. | n.d. | 0.01 | 0.05 | n.d. | n.d. | n.d. | n.d. | n.d. |
| Total | 95.64 | 95.21 | 96.00 | 95.50 | 95.93 | 99.78 | 99.98 | 97.70 | 96.93 | 97.13 | 97.25 | 98.06 |
| Si | 5.37 | 5.41 | 5.52 | 5.45 | 5.59 | 1.41 | 1.45 | 5.06 | 5.02 | 5.04 | 5.05 | 5.08 |
| Ti | 0.57 | 0.64 | 0.60 | 0.66 | 0.27 | 0.00 | 0.01 | 0.00 | 0.00 | 0.00 | 0.00 | 0.00 |
| Al | 2.92 | 2.82 | 2.65 | 2.73 | 2.96 | 9.11 | 9.05 | 3.92 | 3.94 | 3.92 | 3.91 | 3.85 |
| Cr | 0.01 | 0.00 | 0.00 | 0.00 | 0.01 | 0.00 | 0.00 | 0.00 | 0.00 | 0.00 | 0.00 | 0.00 |
| $Fe^{2+}$ | 1.90 | 2.14 | 2.47 | 1.89 | 0.69 | 0.39 | 0.43 | 0.52 | 0.51 | 0.47 | 0.49 | 0.17 |
| $Fe^{3+}$ | n.c. | n.c. | n.c. | n.c. | n.c. | 0.08 | 0.04 | n.c. | n.c. | n.c. | n.c. | n.c. |
| Mg | 2.84 | 2.55 | 2.28 | 2.82 | 4.26 | 2.99 | 3.00 | 1.47 | 1.52 | 1.55 | 1.52 | 1.87 |
| Mn | 0.01 | 0.00 | 0.01 | 0.00 | 0.00 | 0.01 | 0.01 | 0.00 | 0.00 | 0.01 | 0.00 | 0.01 |
| Ca | 0.00 | 0.00 | 0.02 | 0.00 | 0.00 | 0.00 | 0.00 | 0.00 | 0.00 | 0.00 | 0.00 | 0.00 |
| Na | 0.02 | 0.03 | 0.05 | 0.05 | 0.04 | 0.01 | 0.01 | 0.02 | 0.02 | 0.02 | 0.02 | 0.03 |
| K | 1.95 | 1.96 | 1.95 | 1.94 | 1.77 | 0.00 | 0.00 | 0.00 | 0.00 | 0.00 | 0.00 | 0.00 |
| Ba | n.d. | n.d. | 0.01 | n.d. | n.d. | 0.00 | 0.00 | n.d. | n.d. | n.d. | n.d. | n.d. |
| P | n.d. | n.d. | n.d. | n.d. | n.d. | 0.00 | 0.00 | n.d. | n.d. | n.d. | n.d. | n.d. |
| Total | 15.59 | 15.55 | 15.56 | 15.54 | 15.59 | 14.00 | 14.00 | 10.99 | 11.01 | 11.01 | 10.99 | 11.01 |
| Oxygen | 22 | 22 | 22 | 22 | 22 | 20 | 20 | 18 | 18 | 18 | 18 | 18 |
| $X_{Mg}$ | 0.6 | 0.54 | 0.48 | 0.6 | 0.86 | 0.88 | 0.87 | 0.74 | 0.75 | 0.77 | 0.76 | 0.92 |

$Fe^{3+}$ calculated assuming stoichiometry. n.c., not calculated; n.d., not determined. *Core analysis; ‡Rim analysis.

**Table 5.** Representative electron microprobe analyses of metapelitic orthopyroxene, plagioclase, and alkalifeldspar.

| Sample No. | 83-13 Opx (268)* | 83-13 Opx (270)* | 83-13 Opx (45)‡ | 83-13 Opx (31)‡ | 81-1 Opx (536) | 90-1 Pl (442)¶ | 90-1 Pl (444)¶ | 90-1 Pl§ | 90-1 Pl§ | 90-1 Pl (456)¶ | 90-1 Kfs (468) | 90-1 Kfs (495) |
|---|---|---|---|---|---|---|---|---|---|---|---|---|
| $SiO_2$ | 48.81 | 48.21 | 49.45 | 49.11 | 50.01 | 57.42 | 58.04 | 60.17 | 60.38 | 56.25 | 64.06 | 64.44 |
| $TiO_2$ | 0.00 | 0.00 | 0.11 | 0.10 | 0.11 | n.d. | n.d. | n.d. | n.d. | n.d. | n.d. | n.d. |
| $Al_2O_3$ | 7.32 | 8.03 | 6.25 | 6.61 | 4.89 | 26.08 | 25.70 | 24.41 | 24.47 | 27.67 | 18.43 | 18.67 |
| $Cr_2O_3$ | 0.00 | 0.00 | 0.06 | 0.07 | 0.01 | n.d. | n.d. | n.d. | n.d. | n.d. | n.d. | n.d. |
| FeO | 22.80 | 22.72 | 23.48 | 23.52 | 25.05 | n.c. | n.c. | n.c. | n.c. | n.c. | n.c. | n.c. |
| $Fe_2O_3$ | n.c. | n.c. | n.c. | n.c. | n.c. | 0.32 | 0.60 | 0.26 | 0.27 | 0.42 | 0.05 | 0.00 |
| MgO | 20.06 | 19.90 | 20.19 | 20.10 | 19.18 | n.d. | n.d. | n.d. | n.d. | n.d. | n.d. | n.d. |
| MnO | 0.36 | 0.31 | 0.27 | 0.27 | 0.59 | n.d. | n.d. | n.d. | n.d. | n.d. | n.d. | n.d. |
| CaO | 0.05 | 0.03 | 0.02 | 0.06 | 0.04 | 8.36 | 8.14 | 6.41 | 6.42 | 9.84 | 0.04 | 0.14 |
| $Na_2O$ | 0.00 | 0.00 | 0.04 | 0.04 | 0.00 | 6.46 | 6.57 | 7.70 | 7.80 | 5.58 | 1.30 | 1.87 |
| $K_2O$ | 0.00 | 0.00 | 0.01 | 0.01 | 0.00 | 0.60 | 0.41 | 0.23 | 0.21 | 0.28 | 15.36 | 14.15 |
| BaO | n.d. | n.d. | n.d. | n.d. | n.d. | 0.00 | 0.01 | 0.05 | 0.00 | 0.00 | 0.48 | 0.53 |
| Total | 99.40 | 99.20 | 99.88 | 99.89 | 99.88 | 99.24 | 99.47 | 99.23 | 99.55 | 100.04 | 99.72 | 99.80 |
| Si | 1.83 | 1.81 | 1.85 | 1.84 | 1.89 | 2.60 | 2.62 | 2.70 | 2.70 | 2.53 | 2.98 | 2.98 |
| Ti | 0.00 | 0.00 | 0.00 | 0.00 | 0.00 | n.d. | n.d. | n.d. | n.d. | n.d. | n.d. | n.d. |
| Al | 0.32 | 0.36 | 0.28 | 0.29 | 0.22 | 1.39 | 1.37 | 1.29 | 1.29 | 1.47 | 1.01 | 1.02 |
| Cr | 0.00 | 0.00 | 0.00 | 0.00 | 0.00 | n.d. | n.d. | n.d. | n.d. | n.d. | n.d. | n.d. |
| $Fe^{2+}$ | 0.72 | 0.71 | 0.74 | 0.74 | 0.79 | n.c. | n.c. | n.c. | n.c. | n.c | n.c | n.c. |
| $Fe^{3+}$ | n.c. | n.c. | n.c. | n.c. | n.c. | 0.01 | 0.02 | 0.01 | 0.01 | 0.01 | 0.00 | 0.00 |
| Mg | 1.12 | 1.12 | 1.13 | 1.12 | 1.08 | n.d. | n.d. | n.d. | n.d. | n.d. | n.d. | n.d. |
| Mn | 0.01 | 0.01 | 0.01 | 0.01 | 0.02 | n.d. | n.d. | n.d. | n.d. | n.d. | n.d. | n.d. |
| Ca | 0.00 | 0.00 | 0.00 | 0.00 | 0.00 | 0.41 | 0.39 | 0.31 | 0.31 | 0.47 | 0.00 | 0.01 |
| Na | 0.00 | 0.00 | 0.00 | 0.00 | 0.00 | 0.57 | 0.57 | 0.67 | 0.68 | 0.49 | 0.12 | 0.17 |
| K | 0.00 | 0.00 | 0.00 | 0.00 | 0.00 | 0.04 | 0.02 | 0.01 | 0.01 | 0.02 | 0.91 | 0.84 |
| Ba | n.d. | n.d. | n.d. | n.d. | n.d. | 0.00 | 0.00 | 0.00 | 0.00 | 0.00 | 0.01 | 0.01 |
| Total | 4.00 | 4.01 | 4.01 | 4.00 | 4.00 | 5.02 | 4.99 | 4.99 | 5.00 | 4.99 | 5.03 | 5.03 |
| Oxygen | 6 | 6 | 6 | 6 | 6 | 8 | 8 | 8 | 8 | 8 | 8 | 8 |
| $X_{Mg}$ | 0.61 | 0.61 | 0.60 | 0.60 | 0.58 | – | – | – | – | – | – | – |
| $X_{Ab}$ | – | – | – | – | – | 0.56 | 0.58 | 0.68 | 0.68 | 0.50 | 0.11 | 0.16 |
| $X_{An}$ | – | – | – | – | – | 0.40 | 0.40 | 0.31 | 0.31 | 0.48 | 0.00 | 0.01 |
| $X_{Or}$ | – | – | – | – | – | 0.04 | 0.02 | 0.01 | 0.01 | 0.02 | 0.89 | 0.83 |

In feldspar all iron as $Fe^{3+}$. n.c., not calculated; n.d., not determined. *Core analysis; ‡rim analysis; ¶inclusion in Grt; §matrix.

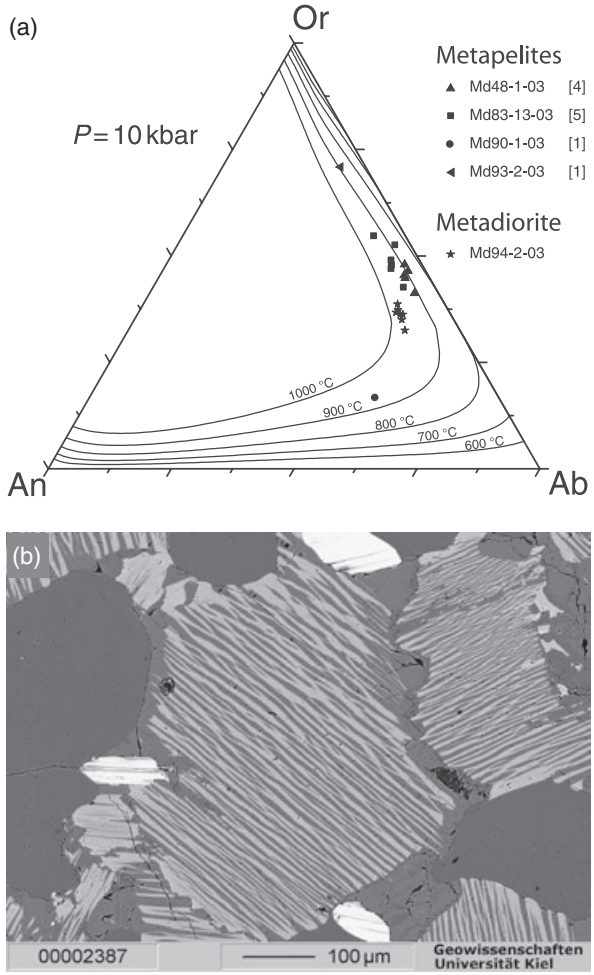


**Fig. 7.** (a) Results of the feldspar thermometry. Most reintegrated compositions of mesoperthites give temperatures in the range of 900–1000 °C. Isopleths after Fuhrmann & Lindsley (1988). Numbers in brackets correspond to mineral assemblages in Table 2. (b) Typical rock texture showing large mesoperthitic feldspar (backscattered electron image).

sion is lower compared with conventional isotopic dating techniques, the advantages of the method are a high spatial resolution (the diameter of measurement points is $< 5$ $\mu$m) and the possibility to perform texturally controlled *in situ* analyses. Compared with conventional analyses, this approach, in combination with careful studies of backscattered electron images and X-ray maps of the analysed monazite, can avoid the danger of determining geologically meaningless mixed ages between different metamorphic events.

### Monazite textures and chemistry

Monazite occurs evenly distributed in metapelitic rocks. It is typically between 10 and 250 $\mu$m in size, and in backscattered electron images, it generally shows a homogeneous core ($M_1$) and a narrow rim ($M_2$; Fig. 9a,b). In rare cases, a distinct part of the core shows an additional magmatic zonation pattern ($M_0$; Fig. 9c). Monazite included in garnet often has more irregular shapes than matrix monazite and shows no distinguishable rim (Fig. 9d). Patchy zonation patterns are just rarely observed. Monazite shows the characteristic LREE enrichment over HREE (Fig. 10; representative analyses in Table 8), as it is typical in garnet-bearing rocks (Zhu & O'Nions, 1999). As regards end-members, they are chemically characterized as $X_{\mathrm{LREE}} = 0.67$–$0.95$, $X_{\mathrm{HREE}} = 0.00$–$0.06$, $X_{\mathrm{Hut}} = 0.00$–$0.07$, $X_{\mathrm{Brb}} = 0.00$–$0.17$ and $X = 0.00$–$0.35$ (calculation described in Pyle *et al.*, 2001). Maximum $Y_2O_3$ content is 5.5 wt%, and $ThO_2$ is in the range from 3 to 18 wt%. The rims are antithetically composed, i.e. higher amounts of Th are correlated with lower amounts of Y. The Y-poor rims point to previous extensive garnet crystallization, which has a strong influence over Y and HREE contents of monazite. Differences in Th content may be related to coexisting zircon (Pyle *et al.*, 2001), which has been found to occur as well. Rims also show a high variation in the

**Table 6.** Summary of representative *P–T* calculations.

| | Sample | Combination | | Temp. (°C) | Press. (kbar) |
|---|---|---|---|---|---|
| progr. | Md90-1-03 | Grt334*/Pl442 | GASP | (550) | 6.1 |
| | | Grt336*/Pl444 | GASP | (550) | 6 |
| | Md90-1-03 | Grt40*/Pl456¶/Mnz265/Ap23 | Grt-Mnz | 582 | (6.0) |
| | | Grt12*/Pl456¶/Mnz265/Ap23 | Grt-Mnz | 563 | (6.0) |
| peak | Md90-1-03 | Grt411†/Pl462*S* | GASP | (950) | 9.3 |
| | | Grt412†/Pl461*S* | GASP | (950) | 8.9 |
| | Md83-13-03 | Grt89*/Opx268* | Al-in-Opx | 989 | (9.0) |
| | | Grt96*/Opx270* | Al-in-Opx | 1009 | (9.0) |
| retro. 1 | Md82-2-03 | Grt29†/Crd20*S* | Grt-Crd-Sil-Qtz | (850) | 5.8 |
| | | Grt774†/Crd826*S* | Grt-Crd-Sil-Qtz | (850) | 6.4 |
| | Md83-13-03 | Grt39†/Opx45† | Al-in-Opx | 823 | (6.0) |
| | | Grt49†/Opx31‡ | Al-in-Opx | 883 | (6.0) |
| retro. 2 | Md84-1-03 | Grt776‡/Crd819‡ | Grt-Crd (Fe-Mg) | 643 | (6.0) |
| | | Grt774‡/Crd823‡ | Grt-Crd (Fe-Mg) | 663 | (6.0) |

All samples are metapelites from the area around Andapa. Pressure and temperature values in parentheses are assumed values for calculation.
GASP: Koziol (1989); Grt-Mnz: Pyle *et al.* (2001); Al-in-Opx: Harley & Green (1982); Grt-Crd-Sil-Qtz & Grt-Crd (Fe-Mg): Berman (1991) with Berman & Aranovich (1996).
*Core analysis; †outer zone analysis; ‡rim analysis; ¶inclusion in Grt; §matrix.

**Table 7.** Examples of reintegrated feldspar compositions as well as compositions and proportions of hosts and exsolution lamellae from three metapelitic and one meta-igneous sample.

| Sample | Rock type* | Vol.% | Pl composition | Vol.% | Kfs composition | Integrated composition |
|---|---|---|---|---|---|---|
| Md48-1-03 | Metapelite [4] | 48.3 | $Ab_{0.92}An_{0.07}Or_{0.01}$ | 51.7 | $Ab_{0.07}An_{0.00}Or_{0.93}$ | $Ab_{0.49}An_{0.04}Or_{0.47}$ |
| Md83-13-03 | Metapelite [5] | 39.3 | $Ab_{0.83}An_{0.16}Or_{0.01}$ | 60.7 | $Ab_{0.22}An_{0.01}Or_{0.77}$ | $Ab_{0.46}An_{0.07}Or_{0.47}$ |
| Md90-1-03 | Metapelite [1] | 18.1 | $Ab_{0.68}An_{0.31}Or_{0.01}$ | 81.9 | $Ab_{0.11}An_{0.00}Or_{0.89}$ | $Ab_{0.58}An_{0.25}Or_{0.17}$ |
| Md93-2-03 | Metapelite [1] | 21.4 | $Ab_{0.76}An_{0.23}Or_{0.01}$ | 78.6 | $Ab_{0.10}An_{0.00}Or_{0.90}$ | $Ab_{0.24}An_{0.05}Or_{0.71}$ |
| Md94-2-03 | Metadiorite | 61.1 | $Ab_{0.82}An_{0.17}Or_{0.01}$ | 38.9 | $Ab_{0.10}An_{0.00}Or_{0.90}$ | $Ab_{0.54}An_{0.11}Or_{0.35}$ |

*Number in parentheses correspond to assemblage number in Table 2.

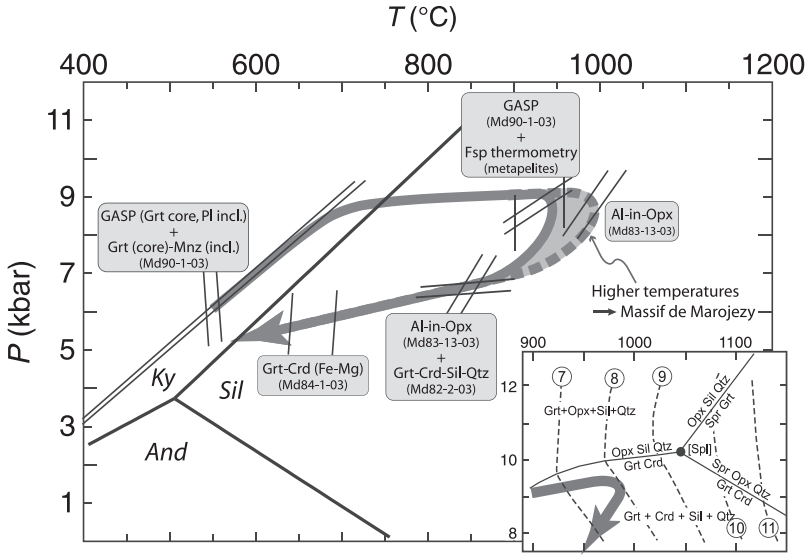


**Fig. 8.** Pressure–temperature diagram depicting the metamorphic evolution of the southern Bemarivo Belt, as deduced from conventional geothermobarometry of metapelitic rocks. The inset shows the isopleths of $Al_2O_3$ in orthopyroxene (wt%, encircled numbers) in the assemblages Grt-Opx-Sil-Qtz and Grt-Crd-Sil-Qtz (after Harley & Motoyoshi, 2000). Orthopyroxene with 8 wt% $Al_2O_3$ corresponds to temperatures of *c*. 970 °C.

amount of lead (0.1–0.4 wt% PbO). The chondrite-normalized REE + Y distribution patterns are mostly similar, and a negative Eu anomaly is always present (Fig. 10). Comparing all monazite analyses, magmatically zoned cores ($M_0$) have chondrite-normalized elemental ratios $(La/Nd)_N$ of 4.0–4.6, whereas other analyses give lower values ($M_1$: 2.1–3.75; $M_2$: 1.5–2.7). Moreover, $(La/Sm)_N$ differs significantly from magmatic cores (11.2–17.7) to $M_1$ (5.8–9.8) and $M_2$ (3.5–7.8). The Eu/Eu* ($Eu_N/\sqrt{Sm_N \cdot Gd_N}$) shows just a slight variation from 0.02 to 0.18 in magmatic and $M_1$ monazite, but $M_2$ rims mostly have Eu contents below the detection limit (Fig. 10a–c). Aside from these general observations, the chemical characteristics of monazite are to some degree also influenced by local mineral equilibria.

The observations that the rims have a slightly different chemistry and that monazite inclusions in garnet do not show this rim, let us conclude that metamorphic growth took place during two phases. The first phase was before and during garnet growth, and the second may be related to the peak-metamorphic stage and the retrograde path. Unfortunately, no textures that help to assign the different zones to specific monazite-forming reactions have been found. However, in the sample used for garnet-monazite thermometry (Md90-1-03), apatite is just found as inclusions in garnet, but it is absent in the matrix of the rock, pointing to the growth of monazite at the expense of apatite. Narrow monazite rims have also been observed elsewhere (Braun *et al*., 1998; de Wit *et al*., 2001; Santosh *et al*., 2005), where they are interpreted as either due to diffusive Pb loss or late-stage hydrothermal interaction or recrystallization during a later metamorphic event. It has been demonstrated by Cherniak *et al*. (2004) that diffusive Pb loss plays no significant role, but an origin of the rims from recrystallization or hydrothermal interaction cannot be excluded. However, such a recrystallization would be expected to take place during the peak or the retrograde stage of metamorphism, leaving our interpretation uninfluenced.

## Geochronological results

Six samples from six localities were analysed, covering the whole southern part of the Bemarivo Belt: sample Md48-1-03 from the Sambirano river; samples Md82-2-03, Md83-12-03, Md83-13-03, Md84-1-03 and Md90-1-03 from the Andapa region. The results are given in Table 9 and Fig. 11. Magmatic ($M_0$) ages are rarely preserved by a few apparent ages in the range from 640 to 850 Ma. The best estimate for $M_0$ can be made from the sample Md83-13-03, where four analyses vary in their $ThO_2^*$ from ~3 to 15 wt%, giving 737 ± 19 Ma (Fig. 11d). Because of our observation that metamorphic monazite mostly shows two-stage growth textures ($M_1$ & $M_2$), measurements from

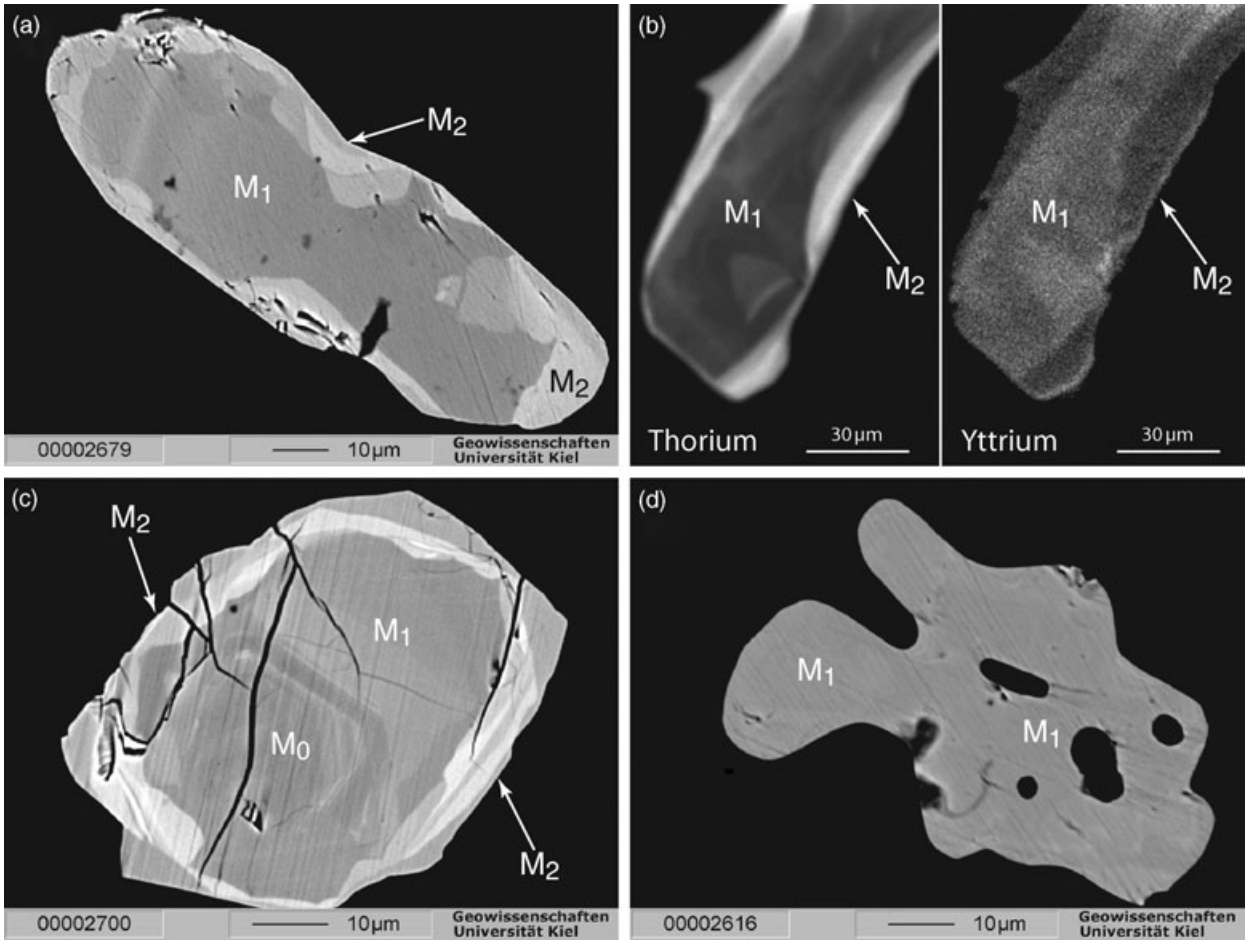


**Fig. 9.** Monazite from metapelites of the southern Bemarivo Belt, and the correlation of growth zones with magmatic ($M_0$) as well as two metamorphic stages ($M_1$ & $M_2$). (a) Monazite with a homogeneous core ($M_1$) and an overgrown $M_2$ rim (backscattered electron image; Md83-12-03). (b) X-ray maps for Th and Y. $M_2$ rims are Th-rich but poor in Y (lighter colours correspond to higher concentrations; Md90-1-03). (c) Monazite with a magmatic core ($M_0$), a metamorphic core ($M_1$), and an overgrown $M_2$ rim (backscattered electron image; Md83-13-03). (d) Irregularly shaped monazite inclusion ($M_1$) in garnet, showing no younger rim (backscattered electron image; Md82-2-03).

both the cores and the rims were evaluated separately. Isochron ages for the $M_1$ stage of metamorphism are in the range from 563 ± 28 Ma to 532 ± 23 Ma, whereas the $M_2$ stage gives slightly lower results from 521 ± 25 Ma to 513 ± 14 Ma (Table 8). These results are overlapping within their $2\sigma$ errors, nonetheless because of textural and chemical differences, it is considered to be likely that both represent true metamorphic ages. Although precision is poor, they indicate a timeframe of *c*. 18–44 Myr from prograde garnet formation to peak metamorphism and cooling.

## DISCUSSION AND CONCLUSIONS

### *P–T* path and geodynamic interpretation

Magmatic ages of *c*. 715 Ma (Tucker *et al*., 1999a) in the Série de Daraina-Milanoa and 753.8 ± 1.7 Ma (Tucker *et al*. in Ashwal, 1997) from the granites of the central Bemarivo Belt are known, but have never been reported from the Série de Sahantaha. U-Pb dating of zircon from the Antananarivo Block (Tucker *et al*., 1999b; Kröner *et al*., 2000) also revealed a period of granitoid magmatism in the middle Neoproterozoic (825–640 Ma). Although we have not dated zircon, which is a common detrital mineral, the magmatic zonation patterns found in monazite of a metapelite let us conclude that within the cores of some grains relics of detrital monazite were preserved, and therefore point to 737 ± 19 Ma as a maximum age for sedimentation. Their host rock may originate from the Neoproterozoic continental arc, the relics of which are assumed to be found in the northern Bemarivo Belt and in the Seychelles (Tucker *et al*., 1999a; Buchwaldt & Tucker, 2001). An origin in the Antananarivo Block is less likely, but cannot be excluded. After erosion and transport, the Série de Sahantaha was deposited. Dur-

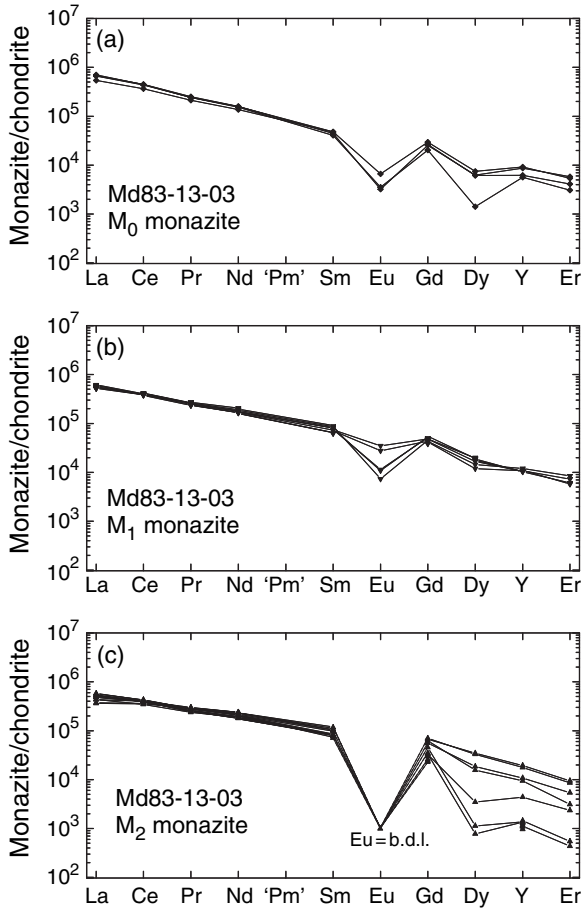


**Fig. 10.** Chondrite-normalized REE + Y distribution patterns of monazite analyses from a metapelitic sample (Md83-13-03; 6 monazite grains). There are no clear differences in chemistry between magmatically zoned cores (a) and metamorphic cores (b). Metamorphically overgrown rims (c) have Eu values below the limit of detection (arbitrarily fixed in the diagram). Normalization values taken from McDonough & Sun (1995).

**Table 8.** Representative electron microprobe analyses of monazite of all three generations: magmatic (no. 195), $M_1$ (no. 78 and 265), and $M_2$ (no. 72).

| Sample | 83-13 | 83-12 | 90-1 | 83-12 |
|---|---|---|---|---|
| No. | 195 | 78 | 265 | 72 |
| $P_2O_5$ | 30.75 | 29.85 | 29.45 | 29.92 |
| $SiO_2$ | 0.21 | 0.27 | 0.53 | 0.61 |
| CaO | 0.53 | 0.85 | 1.58 | 1.35 |
| $Y_2O_3$ | 1.73 | 1.61 | 1.65 | 0.40 |
| $La_2O_3$ | 18.79 | 14.39 | 13.14 | 13.26 |
| $Ce_2O_3$ | 32.12 | 28.64 | 26.30 | 27.26 |
| $Pr_2O_3$ | 2.74 | 3.16 | 2.85 | 3.02 |
| $Nd_2O_3$ | 8.45 | 11.97 | 11.23 | 11.87 |
| $Sm_2O_3$ | 0.77 | 2.10 | 1.83 | 2.55 |
| $Eu_2O_3$ | 0.02 | 0.11 | 0.00 | b.d.l. |
| $Gd_2O_3$ | 0.58 | 1.75 | 1.53 | 2.12 |
| $Dy_2O_3$ | 0.18 | 0.46 | 0.46 | 0.15 |
| $Er_2O_3$ | 0.11 | 0.05 | 0.09 | b.d.l. |
| PbO | 0.12 | 0.13 | 0.22 | 0.25 |
| $ThO_2$ | 2.77 | 4.02 | 8.66 | 6.54 |
| $UO_2$ | 0.20 | 0.40 | 0.25 | 1.42 |
| $Al_2O_3$ | b.d.l. | 0.01 | 0.01 | 0.02 |
| Total | 100.07 | 99.77 | 99.78 | 99.74 |
| P | 1.004 | 0.991 | 0.979 | 0.973 |
| Si | 0.008 | 0.010 | 0.021 | 0.024 |
| Ca | 0.022 | 0.036 | 0.067 | 0.057 |
| Y | 0.036 | 0.034 | 0.035 | 0.008 |
| La | 0.267 | 0.208 | 0.190 | 0.194 |
| Ce | 0.454 | 0.411 | 0.378 | 0.397 |
| Pr | 0.038 | 0.045 | 0.041 | 0.044 |
| Nd | 0.116 | 0.168 | 0.158 | 0.168 |
| Sm | 0.010 | 0.028 | 0.025 | 0.035 |
| Eu | 0.000 | 0.002 | 0.000 | b.d.l. |
| Gd | 0.007 | 0.023 | 0.020 | 0.028 |
| Dy | 0.002 | 0.006 | 0.006 | 0.002 |
| Er | 0.001 | 0.001 | 0.001 | b.d.l. |
| Pb | 0.001 | 0.001 | 0.002 | 0.003 |
| Th | 0.024 | 0.036 | 0.077 | 0.059 |
| U | 0.002 | 0.004 | 0.002 | 0.013 |
| Al | b.d.l. | 0.000 | 0.001 | 0.001 |
| Total | 1.992 | 2.004 | 2.002 | 2.005 |
| $X_{LREE}$ | 0.902 | 0.859 | 0.790 | 0.831 |
| $X_{HREE}$ | 0.011 | 0.029 | 0.027 | 0.030 |
| $X_{Hut}$ | 0.006 | 0.006 | 0.016 | 0.017 |
| $X_{Brb}$ | 0.045 | 0.072 | 0.133 | 0.114 |
| $X_{YPO4}$ | 0.036 | 0.034 | 0.034 | 0.008 |
| App. age | 817 ± 29 | 563 ± 19 | 545 ± 12 | 514 ± 10 |

Cations calculated on the basis of 4 oxygen.
The apparent age is given in Ma with $2\sigma$ error.

ing the amalgamation of Gondwana, the continental arc may have collided with the already consolidated continental fragments of Gondwana, i.e. the Antongil Block, the Indian Dharwar craton, and the Antananarivo Block. The collision and overthrusting led to burial of the Série de Sahantaha to a depth of $>25$ km and its syntectonic metamorphism. It is possible that the Série de Daraina-Milanoa in the northern Bemarivo Belt was also affected by this tectonism, but buried to lower depth and therefore overprinted to lower-metamorphic grades of just 500–600 °C. The burial of the Série de Sahantaha was followed by heating to temperatures of ~900–950 °C, locally even reaching higher temperatures of nearly 1000 °C. Such ultrahigh temperatures are likely to be caused by magma intrusions into the thickened lower crust. The large charnockite complexes in the southern Bemarivo Belt may represent such intrusive bodies delivering the heat for high-$T$ metamorphism. Decompression took also place under high-$T$ conditions, as deduced from the extensive late-stage formation of broad cordierite rims around garnet. There are two main tectonothermal models for isothermal decompression following crustal thickening: extensional tectonics leading to tectonic denudation (e.g. Ridley, 1989) or prolonged transpression causing extrusion of the lower crust (e.g. Thompson *et al.*, 1997; Schulmann *et al.*, 2002). Up to now, structural data are lacking for the studied area. Therefore none of these models can be excluded. Although cordierite-bearing assemblages in the Sambirano area of the Série de Sahantaha have not been found, the occurrence of charnockites, mesoperthitic feldspar in metasediments, and the chemistry of biotite is consistent with the metamorphic conditions deduced from the metapelites of the Andapa region more to the east. However, peak-pressure estimates in the Sambirano area are lacking because of missing suitable assemblages. It has to be

**Table 9.** Results of monazite dating for six metapelitic samples.

| Sample: | Md48-1-03 | Md82-2-03 | Md83-12-03 | Md83-13-03 | Md84-1-03 | Md90-1-03 |
|---|---|---|---|---|---|---|
| No. of monazite: | 5 | 5 | 7 | 6 | 8 | 5 |
| n (M0) | – | – | – | 4 | – | 4 |
| Age (M0) | – | – | – | 737 ± 19 Ma | – | 770 ± 219 Ma |
| MSWD (M0) | – | – | – | 0.9479 | – | 1.9753 |
| n (M1) | 21 | 47 | 21 | 33 | 73 | 17 |
| Age (M1) | 547 ± 40 Ma | 532 ± 23 Ma | 543 ± 21 Ma | 550 ± 38 Ma | 563 ± 28 Ma | 538 ± 17 Ma |
| MSWD (M1) | 0.7311 | 0.7705 | 0.6296 | 0.7602 | 1.0093 | 0.4498 |
| n (M2) | 12 | 15 | 18 | 17 | 9 | 23 |
| age (M2) | 521 ± 25 Ma | 513 ± 14 Ma | 518 ± 25 Ma | 512 ± 18 Ma | 519 ± 29 Ma | 520 ± 13 Ma |
| MSWD (M2) | 0.8231 | 0.5588 | 0.4996 | 0.381 | 0.1481 | 0.4989 |

Given are the number of measurement points used for age calculation (n), the age (errors are $2\sigma$), and the MSWD of the isochron line. Ages for magmatic ($M_0$), as well as two metamorphic stages ($M_1$ and $M_2$) have been calculated separately.

mentioned that the variation in mineral chemistry seen in samples of the Andapa area must not stringently be due to a general increase in metamorphic conditions in the whole southern Bemarivo Belt from east to west (as proposed by Hottin, 1976). Possibly, the observed regional systematic change in mineral chemistry reflects the local influence of the Massif de Marojezy, delivering heat and causing higher metamorphic temperatures.

### Interpretation of the geochronological results

Monazite ages, as well as peak-temperature conditions, are similar in the whole southern Bemarivo Belt, but $M_0$ ages have not been found in the Sambirano area. An age of 737 ± 19 Ma is consistent with known magmatic ages from the northern Bemarivo Belt and therefore considered as the age of the detritus-delivering source rocks. Interpreting the geochronological results of $M_1$ cores and $M_2$ rims of monazite, which differ 18–44 Myr in age, the results of Buchwaldt *et al.* (2003) have to be considered. These authors performed conventional U/Pb geochronology, and dated the metamorphism with single pelitic monazite grains at 519.2 ± 0.7 Ma and 520 ± 1 Ma. Titanite from metapelitic granulites gave 511 ± 5 Ma and zircon from the Massif de Marojezy is 520.9 ± 4.2 Ma in age, interpreted as the timing of charnockite emplacement. These geochronological results can be correlated with our $M_2$ results, whereas the $M_1$ ages have not been determined by Buchwaldt *et al.* (2003). The most likely scenario is that the emplacement of the Marojezy charnockite took place at *c.* 521 Ma, causing the high-*T* metamorphism and growth of $M_2$ monazite. The $M_1$ ages (563–532 Ma) date the prograde metamorphic stage, representing the time of crustal thickening.

### The Bemarivo Belt and its relation to the formation of Gondwana

The ages obtained in the Bemarivo Belt are among the youngest for high-grade metamorphism in Madagascar. The metamorphism in southern Madagascar, especially shear zone activity, is of similar age or even younger (Kröner *et al.*, 1996; Montel *et al.*, 1996; Martelat *et al.*, 1999, 2000). Rocks of the famous ultrahigh temperature-metamorphic Andriamena unit (Tsaratanana sheet, north-central Madagascar) show late Neoproterozoic or even Cambrian growth of monazite, interpreted as either due to fluid-assisted resetting or cooling (Goncalves *et al.*, 2003, 2004; Paquette *et al.*, 2004). Similar monazite ages from the Itremo region of central Madagascar are also ascribed to late-stage fluid circulation (Fernandez *et al.*, 2003). Granulite-facies metamorphism in the central Antananarivo Block is believed to date to *c.* 550 Ma, deduced from U-Pb analyses of metamorphically overgrown zircon rims (Kröner *et al.*, 2000) or to 580–520 Ma from lower discordia intercepts (Tucker *et al.*, 1999b). However, estimates for metamorphic conditions in rocks of the Antananarivo Block are not well constrained because of the scarcity of metapelitic rocks. Stratoid granites, which occur frequently and widely distributed in the Antananarivo Block, are interpreted to have formed in a post-collisional extensional setting (Nédélec *et al.*, 1995), and were used to constrain the time of collision with East Africa to *c.* 650 Ma (Paquette & Nédélec, 1998), which would be much older than the collisional event in the Bemarivo Belt. In contrast, the high-grade metamorphism in Tanzania is of similar age (650–620 Ma), but is interpreted to result from magmatic underplating (Appel *et al.*, 1998; Möller *et al.*, 2000) preceding the collisional event, which occurred at *c.* 540 Ma (A. Möller pers. comm.; see discussion in Jöns & Schenk, 2004). Other interpretations consider the collisional event at *c.* 650 Ma, followed by *c.* 550 Ma post-collisional extension and shearing (Stern, 1994; Meert *et al.*, 1995; Meert, 2003). However, these interpretations are not based on correlations of metamorphic *P–T* paths with radiometric ages. In this context, the timing of the collision in Madagascar also remains debateable. A partial overthrusting of the Bemarivo Belt onto the already consolidated Antananarivo Block and Antongil Block has been assumed by Collins *et al.* (2000a), and therefore collision and syntectonic metamorphism

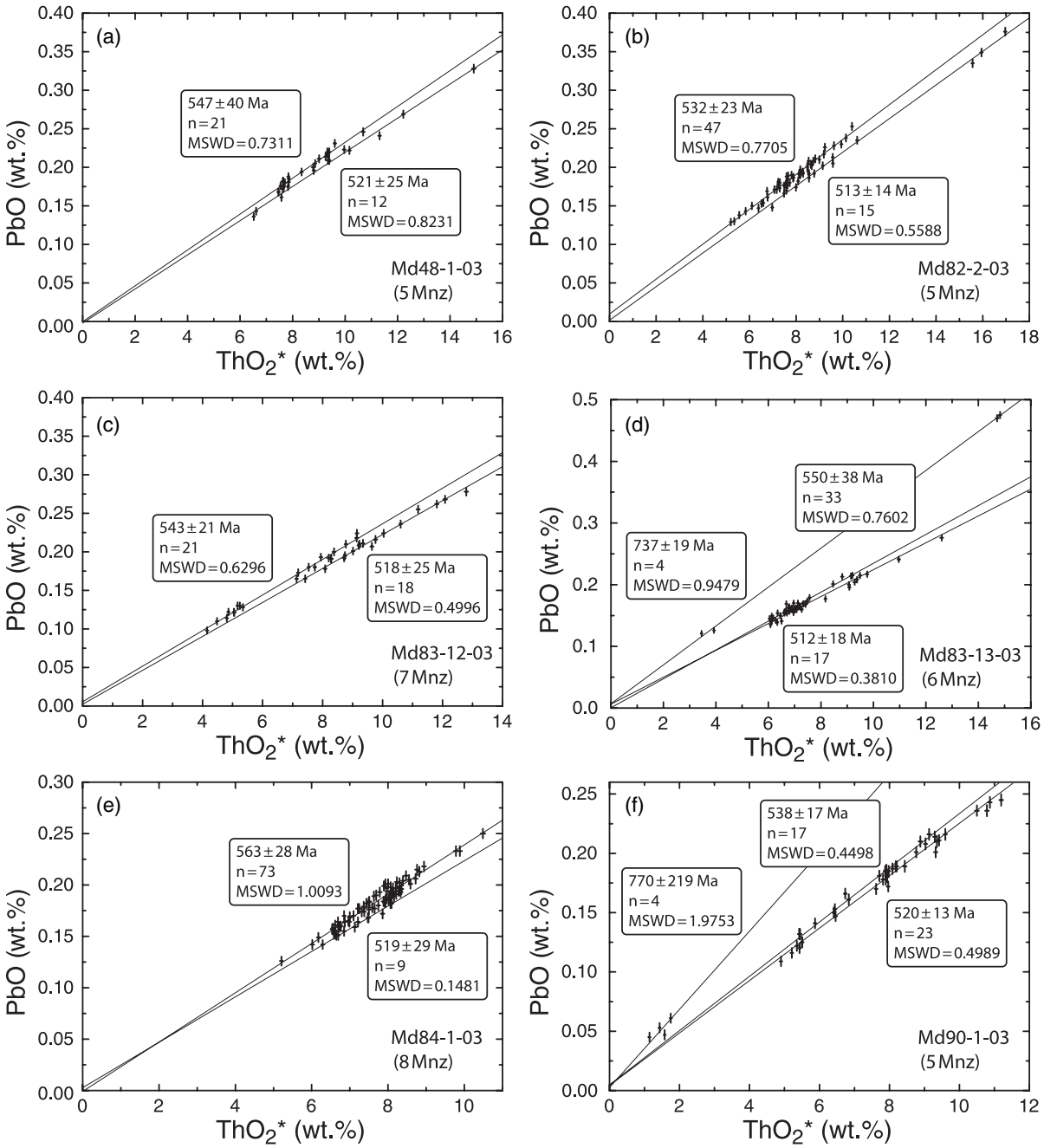


**Fig. 11.** $ThO_2^*$ *v*. PbO diagrams showing isochrons plotted for distinct parts of monazite grains, i.e. cores and rims have been evaluated separately. Rims generally display a larger variation in $ThO_2^*$ values. Just in rare cases (Md83-13-03, Md90-1-03) older magmatic cores are preserved (symbol sizes correspond to analytical uncertainty).

is a conclusive scenario. This collision represents a stage of the final assembly of the Gondwana supercontinent, when the proposed Betsimisaraka suture zone (Kröner *et al*., 2000) of eastern Madagascar may already have been closed. The collision in western Madagascar may also fall into this time period, but detailed study of the metamorphic history of the Antananarivo Block is needed to get a more conclusive picture for both Madagascar and East Africa.

## ACKNOWLEDGEMENTS

We thank B. Mader for her help with the microprobe analyses and A. Fehler for producing the thin sections. Thorough reviews of J.-E. Martelat and R. Buchwaldt helped to improve the manuscript and are kindly acknowledged. D. Robinson is thanked for his careful editorial work. N. Jöns is grateful to the German Academic Exchange Service (DAAD) and the Stu-

dienstiftung des deutschen Volkes (German National Academic Foundation) for financial support. The Deutsche Forschungsgemeinschaft (DFG) supported the project through grants Sche 256/16-1 and Sche 256/17-1.

## REFERENCES


Appel, P., Möller, A. & Schenk, V., 1998. High-pressure granulite facies metamorphism in the Pan-African belt of eastern Tanzania: P-T-t evidence against granulite formation by continent collision. *Journal of Metamorphic Geology*, **16,** 491–509.

Armstrong, J. T., 1995. CITZAF: a package of correction programs for the quantitative electron microbeam X-ray analysis of thick polished materials, thin films, and particles. *Microbeam Analysis*, **4,** 177–200.

Ashwal, L. D., 1997. *Proterozoic Geology of Madagascar: Guidebook to Field Excursions*. Technical report, Gondwana Research Group, Misc. Publications, Osaka.

Berman, R. G., 1991. Thermobarometry using multiequilibrium calculations: a new technique with petrologic applications. *Canadian Mineralogist*, **29,** 833–855.

Berman, R. G. & Aranovich, L. Y., 1996. Optimized standard state and solution properties of minerals I. Model calibration for Olivine, orthopyroxene, cordierite, garnet, and ilmenite in the system MgO-FeO-MgO-CaO-$Al_2O_3$-$TiO_2$-$SiO_2$. *Contributions to Mineralogy and Petrology*, **126,** 1–24.

Besairie, H., 1970. *Description géologique du massif ancien de Madagascar: Centre Nord et Nord-Est*. Documentation du Bureau géologique Numéro 177a, Republique Malagasy, Service géologique, Madagascar.

Braun, I., Montel, J. M. & Nicollet, C., 1998. Electron microprobe dating of monazites from high-grade gneisses and pegmatites of the Kerala Khondalite Belt, southern India. *Chemical Geology*, **146,** 65–85.

Buchwaldt, R. & Tucker, R. D., 2001. P-T-time constraints on the metamorphic rocks of North Madagascar and their relevance on the assembly of Gondwanaland. *Geological Society of America Abstracts with Programs*, **33,** 436.

Buchwaldt, R., Tucker, R. D. & Dymek, R. F., 2003. Geothermobarometry and U-Pb geochronology of metapelitic granulites and pelitic migmatites from the Lokoho region, Northern Madagascar. *American Mineralogist*, **88,** 1753–1768.

Cherniak, D. J., Watson, E. B., Grove, M. & Harrison, T. M., 2004. Pb diffusion in monazite: a combined RBS/SIMS study. *Geochimica et Cosmochimica Acta*, **68,** 829–840.

Cocherie, A., Legendre, O., Peucat, J. J. & Kouamelan, A. N., 1998. Geochronology of polygenetic monazites constrained by in situ electron microprobe Th-U-total lead determination: implications for lead behaviour in monazite. *Geochimica et Cosmochimica Acta*, **62,** 2475–2497.

Collins, A. S. & Windley, B. F., 2002. The tectonic evolution of Central and Northern Madagascar and its place in the final assembly of Gondwana. *The Journal of Geology*, **110,** 325–339.

Collins, A. S., Kröner, A., Razakamanana, T. & Windley, B. F., 2000a. The tectonic architecture and the East African Orogen in central Madagascar: a structural and geochronological perspective. *Journal of African Earth Sciences*, **30,** 21.

Collins, A. S., Razakamanana, T. & Windley, B. F., 2000b. Neoproterozoic extensional detachment in central Madagascar: implications for the collapse of the East African Orogen. *Geological Magazine*, **137,** 39–51.

Fernandez, A., Schreurs, G., Villa, I. M., Huber, S. & Rakotondrazafy, M. A. F., 2003. Age constraints on the tectonic evolution of the Itremo region in Central Madagascar. *Precambrian Research*, **123,** 87–110.

Fitzsimons, I. C. W. & Harley, S. L., 1994. The influence of retrograde exchange on granulite P-T estimates and a convergence technique for the recovery of peak metamorphic conditions. *Journal of Petrology*, **35,** 543–576.

Fuhrmann, M. L. & Lindsley, D. H., 1988. Ternary-feldspar modelling and thermometry. *American Mineralogist*, **73,** 201–215.

Goncalves, P., Nicollet, C. & Lardeaux, J.-M., 2003. Finite strain pattern in Andriamena unit (north-central Madagascar): evidence for late Neoproterozoic-Cambrian thrusting during continental convergence. *Precambrian Research*, **123,** 135–157.

Goncalves, P., Nicollet, C. & Montel, J.-M., 2004. Petrology and in situ U-Th-Pb monazite geochronology of ultrahigh-temperature metamorphism from the Andriamena mafic unit, North-Central Madagascar. Significance of a petrographical P-T path in a polymetamorphic context. *Journal of Petrology*, **45,** 1923–1957.

Harley, S. L. & Green, D. H., 1982. Garnet-orthopyroxene barometry for granulites and peridotites. *Nature*, **300,** 697–701.

Harley, S. L. & Motoyoshi, Y., 2000. Al zoning in orthopyroxene in a sapphirine quartzite: evidence for >1120 °C UHT metamorphism in the Napier Complex, Antarctica, and implications for the entropy of sapphirine. *Contributions to Mineralogy and Petrology*, **138,** 293–307.

Higgins, J. B., Ribbe, P. H. & Herd, R. K., 1979. Sapphirine I: crystal chemical contributions. *Contributions to Mineralogy and Petrology*, **68,** 349–356.

Hottin, G., 1976. Présentation et essai d'interprétation du Précambrien de Madagascar. *Bulletin du Bureau de Recherches géologiques et minière*, **2,** 117–153.

Jarosewich, E. & Boatner, L. A., 1991. Rare-earth element reference samples for electron microprobe analysis. *Geostandards Newsletter*, **15,** 397–399.

Jöns, N. & Schenk, V., 2004. Petrology of whiteschists and associated rocks at Mautia Hill (Tanzania): fluid infiltration during high-grade metamorphism? *Journal of Petrology*, **45,** 1959–1981.

Käse, H. & Metz, P., 1980. Experimental investigation of the metamorphism of siliceous dolomites. *Contributions to Mineralogy and Petrology*, **73,** 151–159.

Kato, T., Suzuki, K. & Adachi, M., 1999. Computer program for the CHIME age calculation. *The Journal of Earth and Planetary Sciences, Nagoya University*, **46,** 49–56.

Kelsey, D. E., White, R. W. & Powell, R., 2005. Calculated phase equilibria in $K_2O$–FeO–MgO–$Al_2O_3$–$SiO_2$–$H_2O$ for silica-undersaturated sapphirine-bearing mineral assemblages. *Journal of metamorphic Geology*, **23,** 217–239.

Koziol, A. M., 1989. Recalibration of the garnet-plagioclase-$Al_2SiO_5$-quartz (GASP) geobarometer and application to natural parageneses. *EOS Transactions*, **70,** 493.

Kretz, R., 1983. Symbols for rock-forming minerals. *American Mineralogist*, **68,** 277–279.

Kröner, A., Braun, I. & Jaeckel, P., 1996. Zircon geochronology of anatectic melts and residues from a high-grade pelitic assemblage at Ihosy, southern Madagascar: evidence for Pan-African granulite metamorphism. *Geological Magazine*, **133,** 311–323.

Kröner, A., Hegner, E., Collins, A. S. *et al.* 2000. Age and magmatic history of the Antananarivo Block, Central Madagascar, as derived from zircon geochronology and Nd isotopic systematics. *American Journal of Science*, **300,** 251–288.

Kusky, T. M., Abdelsalam, M., Tucker, R. D. & Stern, R. J., 2003. Evolution of the East African and related orogens, and the assembly of Gondwana. *Precambrian Research*, **123,** 81–85.

Lacroix, A., 1922. *Minéralogie de Madagascar*, Vols 1–3. Société d'éditions gèographiques, maritimes et coloniales, Paris.

Martelat, J. E., Lardeaux, J. M., Nicollet, C. & Rakotondrazafy, R., 1999. Exhumation of granulites within a transpressive regime; an example from southern Madagascar. *Gondwana Research*, **2,** 363–367.

Martelat, J.-E., Lardeaux, J.-M., Nicollet, C. & Rakotondrazafy, M. A. F., 2000. Strain pattern and late Precambrian deformation history in southern Madagascar. *Precambrian Research*, **102,** 1–20.

McDonough, W. F. & Sun, S. S., 1995. The composition of the Earth. *Chemical Geology*, **120,** 223–253.

McWilliams, M. O., 1981. Palaeomagnetism and Precambrian tectonic evolution of Gondwana. In: *Precambrian Plate Tectonics* (ed. Kröner, A.), pp. 649–687. Elsevier, Amsterdam. Developments in Precambrian Geology.

Meert, J. G., 2003. A synopsis of events related to the assembly of eastern Gondwana. *Tectonophysics*, **362,** 1–40.

Meert, J. G., van der Voo, R. & Ayub, S., 1995. Paleomagnetic investigation of the Neoproterozoic Gagwe lavas and Mbozi Complex, Tanzania and the assembly of Gondwana. *Precambrian Research*, **74,** 225–244.

Möller, A., Mezger, K. & Schenk, V., 2000. U-Pb dating of metamorphic minerals: Pan-African metamorphism and prolonged slow cooling of high pressure granulites in Tanzania, East Africa. *Precambrian Research*, **104,** 123–146.

Montel, J.-M., Veschambre, M. & Nicollet, C., 1994. Datation de la monazite á la microsonde électronique. *Comptes rendus de l'Académie des sciences, Série II*, **318,** 1489–1495.

Montel, J.-M., Foret, S., Veschambre, M., Nicollet, C. & Provost, A., 1996. Electron microprobe dating of monazite. *Chemical Geology*, **131,** 37–53.

Nédélec, A., Stephens, W. E. & Fallick, A. E., 1995. The Panafrican stratoid granites of Madagascar: alkaline magmatism in a post-collisional extensional setting. *Journal of Petrology*, **36,** 1367–1391.

Paquette, J. L. & Nédélec, A., 1998. A new insight into Pan-African tectonics in the East-West Gondwana collision zone by U-Pb zircon dating of granites from central Madagascar. *Earth and Planetary Science Letters*, **155,** 45–56.

Paquette, J. L., Nédélec, A., Moine, B. & Rakotondrazafy, M., 1994. U-Pb, single zircon Pb-evaporation, and Sm-Nd isotopic study of a granulite domain in SE Madagascar. *The Journal of Geology*, **102,** 523–538.

Paquette, J. L., Goncalves, P., Devouard, B. & Nicollet, C., 2004. Micro-drilling ID-TIMS U-Pb dating of single monazites: a new method to unravel complex poly-metamorphic evolutions. Application to the UHT granulites of Andriamena (North-Central Madagascar). *Contributions to Mineralogy and Petrology*, **147,** 110–122.

Parrish, R. R., 1990. U-Pb dating of monazite and its application to geological problems. *Canadian Journal of Earth Sciences (Revue Canadienne des Sciences de la Terre)*, **35,** 1431–1450.

Pyle, J. M., Spear, F. S., Rudnick, R. L. & McDonough, W. F., 2001. Monazite-xenotime-garnet equilibrium in metapelites and a new monazite-garnet thermometer. *Journal of Petrology*, **42,** 2083–2107.

Raase, P. & Schenk, V., 1994. Petrology of granulite-facies metapelites of the Highland Complex, Sri Lanka: implications for the metamorphic zonation and the P-T path. In: *Tectonic, Metamorphic and Isotopic Evolution of Deep Crustal Rocks, with Special Emphasis on Sri Lanka* (eds Raith, M. & Hoernes, S.), pp. 265–294. Elsevier, Amsterdam.

Ridley, J., 1989. Vertical movement in orogenic belts and the timing of metamorphism relative to deformation. In: *Evolution of Metamorphic Belts* (eds Daly, J. S., Cliff, R. A. & Yardley, B. W. D.), pp. 103–115. Geological Society of London Special Publication, London.

Robinson, P., Hollocher, K. T., Tracy, R. J. & Dietsch, C. W., 1982. High grade Acadian regional metamorphism in South-central Massachusetts. In: *Guidebook for fieldtrips in Connecticut and South central Massachusetts* (eds Joesten, R. & Quarrier, S. S.), pp. 289–339. State Geological and Natural History Survey of Connecticut, Storrs.

Santosh, M., Tanaka, K., Yokoyama, K. & Collins, A. S., 2005. Late Neoproterozoic-Cambrian felsic magmatism along transcrustal shear zones in Southern India: U-Pb electron microprobe ages and implications for the amalgamation of the Gondwana supercontinent. *Gondwana Research*, **8,** 31–42.

Schenk, V., 1984. Petrology of felsic granulites, metapelites, metabasics, ultramafics, and metacarbonates from Southern Calabria (Italy): Prograde metamorphism, uplift and cooling of a former lower crust. *Journal of Petrology*, **25,** 255–298.

Schulmann, K., Schaltegger, U., Thompson, A. B. & Edel, J.-B., 2002. Rapid burial and exhumation during orogeny: thickening and synconvergent exhumation of thermally weakened and thinned crust (Variscan Orogen in Western Europe). *American Journal of Science*, **302,** 856–879.

Steiger, R. H. & Jäger, E., 1977. Subcommission on geochronology: convention on the use of decay constants in geo- and cosmochronology. *Earth and Planetary Science Letters*, **36,** 359–362.

Stern, R. J., 1994. Arc assembly and continental collision in the Neoproterozoic East African Orogen: implications for the consolidation of Gondwanaland. *Annual Reviews of Earth and Planetary Sciences*, **22,** 319–351.

Suzuki, K. & Adachi, M., 1991. Precambrian provenance and Silurian metamorphism of the Tsubonosawa paragneiss in the South Kitakami terrane, Northeast Japan, revealed by the chemical Th-U-total Pb isochron ages of monazite, zircon and xenotime. *Geochemical Journal*, **25,** 357–376.

Suzuki, K. & Adachi, M., 1994. Middle Precambrian detrital monazite and zircon from the Hida gneiss in the Oki-Dogo Island, Japan: their origin and implication for the correlation of the basement of Southwest Japan and Korea. *Tectonophysics*, **235,** 277–292.

Thompson, A. B., Schulmann, K. & Jeek, J., 1997. Extrusion tectonics and elevation of lower crustal metamorphic rocks in convergent orogens. *Geology*, **25,** 491–494.

Torsvik, T. H., Carter, L. M., Ashwal, L. D., Bhushan, S. K., Pandit, M. K. & Jamtveit, B., 2001. Rodinia refined or obscured: palaeomagnetism of the Malani Igneous Suite (NW India). *Precambrian Research*, **108,** 319–333.

Tucker, R. D., Ashwal, L. D., Hamilton, M. A., Torsvik, T. H. & Carter, L. M., 1999a. Neoproterozoic silicic magmatism of northern Madagascar, Seychelles, and NW India; clues to Rodinia's assembly and dispersal. *Geological Society of America Abstracts with Programs*, **31,** A317.

Tucker, R. D., Ashwal, L. D., Handke, M. J., Hamilton, M. A., Le Grange, M. & Rambeloson, R. A., 1999b. U-Pb geochronology and isotope geochemistry of the Archean and Proterozoic rocks of North-Central Madagascar. *The Journal of Geology*, **107,** 135–153.

de Wit, M. J., Bowring, S. A., Ashwal, L. D., Randrianasolo, L. G., Morel, V. P. I. & Rambeloson, R. A., 2001. Age and tectonic evolution of Neoproterozoic ductile shear zones in southwestern Madagascar, with implications for Gondwana studies. *Tectonics*, **20,** 1–45.

York, D., 1966. Least-squares fitting of a straight line. *Canadian Journal of Physics*, **44,** 1079–1086.

Zhu, X. K. & O'Nions, R. K., 1999. Monazite chemical compositions: some implications for monazite geochronology. *Contributions to Mineralogy and Petrology*, **137,** 351–363.

*Received 13 July 2005; revision accepted 20 March 2006.*